FLUID HISTORIES OF MIDDLE ORDOVICIAN FAULT-FRACTURE DOLOMITE OIL FIELDS OF THE SOUTHERN MICHIGAN BASIN

By

REGINA F DUNSEITH

Bachelor of Science in Geology and Geophysics

University of Missouri-Rolla

Rolla, Missouri

2009

Submitted to the Faculty of the
Graduate College of the
Oklahoma State University
in partial fulfillment of
the requirements for
the Degree of
MASTER OF SCIENCE
July, 2019

FLUID HISTORIES OF MIDDLE ORDOVICIAN

FAULT-FRACTURE DOLOMITE OIL FIELDS

OF THE SOUTHERN MICHIGAN BASIN

Thesis Approved:

Dr. Jay M. Gregg

Thesis Adviser

Dr. G. Michael Grammer

Dr. Jack Pashin

ACKNOWLEDGEMENTS

This work is the culmination of nearly five years of guidance and aid from many people and organizations. I would like to express my sincerest and humblest thanks to all of them.

Dr. Jay M. Gregg, my advisor and committee chair, for his inspiration for the work, his continuing drive for excellence in research, and ability to help me re-set when I felt overwhelmed. Without his guidance, this paper would not have developed into such a significant work of which I am very proud.

Dr. G. Michael Grammer and Dr. Jack Pashin, my committee members, for their insights, early directions, suggestions, reviews, and ability to connect my work to the broader science.

The Geological Research Laboratory at St. Joe Minerals Corporation for supporting the initial sample collecting and sample preparation for this study, and to Mr. Paul Gerdemann, Vice President of Exploration (Retired), St. Joe Minerals Corporation, for his intellectual contributions to the study.

The Michigan Geological Repository for Research and Education, especially Western Michigan University staff members Dr. William Harrison, Dr. Peter Voice, and Ms. Jennifer Trout, for access to core material, expert guidance in my sampling, and use of the facility.

Funding for this thesis was generously provided by the American Association of Petroleum Geologists Grants-In-Aid Duncan A. McNaughton Memorial and Ohio Geological Society Named Grants, and the Geological Society of America Graduate Student Research Grant program. I am eternally grateful for these organizations and the generous donors who contribute to their grants, which enable student academic research.

My colleagues and co-advisees at Oklahoma State University for their engagement in discussion, and especially Dr. Sahar Mohammadi for training on the equipment and answering technical questions during my research and writing.

Finally, I would like to express my deepest gratitude to my husband, Mark Dunseith, for his unwavering support in all aspects of this journey.

Name: REGINA F DUNSEITH

Date of Degree: JULY, 2019

Title of Study: FLUID HISTORIES OF MIDDLE ORDOVICIAN FAULT-FRACTURE DOLOMITE OIL FIELDS OF THE SOUTHERN MICHIGAN BASIN

Major Field: GEOLOGY

Abstract: Fault-fracture oil fields in the Trenton and Black River formations (TBR) constitute important petroleum reservoirs in the southern Michigan Basin and are the type example for "hydrothermal" petroleum reservoirs world-wide. However, fluid histories of these oil fields are only partially understood.

Petrographic and geochemical data suggest these oil fields evolved as independent fault-controlled convective systems. Homogenization temperatures (T_h) (79º C to 258º C) measured in cement inclusions indicate two fluid endmembers: a warm fluid (<180º C) and a hot fluid (>180º C). The hot fluids appear to only affect oil fields of the south-central Michigan Basin. Decreasing T_h distal from the Proterozoic Mid-Michigan Rift (MMR) suggest that the hot fluids emanated from the rift area. Strontium isotope values indicate two fluid sources: Proterozoic basement and late Silurian evaporites. Values of $^{87}Sr/^{86}Sr$ for cements in the Freedom, Napoleon, Reading, and Scipio fields (0.7086-0.7088) are influenced by warm water sourced from Silurian strata, and values for cements in the Albion, Branch County, and Northville fields (0.7091 to 0.7110) record continental basement signatures.

Included fluids are saline (16.1 to 49.4 wt. % NaCl equivalent) and likely sourced from Silurian Salina Group evaporites. Eutectic temperatures (T_e) (-50º C to -112º C) suggest a complex Na-Ca-KCl brine; the expected composition of dissolved Salina salts. Lower T_e proximal to the MMR suggest the rift as a source of additional complexing cations.

Isotope values for carbonate cements are depleted with respect to $\delta^{18}O$ (-6.59 to -12.46‰ VPDB) relative to Ordovician seawaters, and somewhat depleted with respect to $\delta^{13}C$ (-1.22 to +1.18‰ VPDB). Equilibrium calculations from $\delta^{18}O$ and T_h values indicate cement precipitating waters were highly evolved (+1.3 to +14.4‰ $\delta^{18}O_{VSMOW}$) compared to Ordovician and Silurian seawaters (-5.5‰ $\delta^{18}O_{VSMOW}$).

Cement precipitating fluids in TBR oil fields likely have similar sources and timing. However, water-rock interactions along fault pathways modified source waters, giving each oil field a unique petrographic and geochemical signature. Fluids may have been shared where underlying fault systems are connected and similar cathodoluminescent cement stratigraphies are observed. Reactivation of basement faulting and fluid movement in TBR oil fields likely initiated during Silurian-Devonian tectonism.

TABLE OF CONTENTS

Chapter Page

LIST OF TABLES

LIST OF FIGURES

Figure Page

CHAPTER I

INTRODUCTION

Ordovician dolomites of the southern Michigan Basin have been producing hydrocarbons since 1884 and include some of the largest fields in the Basin, such as the Albion-Scipio trend (Gautier et al., 1995). Producing units are the Trenton and Black River (TBR) Formations of the Middle-Upper Ordovician. Hydrocarbon traps are stratigraphic, formed by non-porous and non-permeable limestone surrounding fault and fracture controlled hydrothermal reservoir dolomites (Grammer and Harrison, 2013). Understanding the processes and fluids involved in creating TBR reservoirs is a key to future exploration and development of the Michigan Basin and can be valuable for understanding and developing other hydrothermal reservoirs.

This study has determined fluid compositions and identified sources of fluids responsible for dolomitization and emplacement of hydrocarbons. Analysis of reservoir cements, including standard thin section and cathodoluminescence (CL) petrography, fluid inclusion microthermometry, and $\delta^{13}C$, $\delta^{18}O$, and $^{87}Sr/^{86}Sr$ isotope geochemistry has been conducted on six fault-fracture hydrothermal oil fields and one non-hydrocarbon productive well in south-central Michigan.

CHAPTER II

GEOLOGIC BACKGROUND

Stratigraphy and Sedimentology

The Michigan Basin is a roughly circular intracratonic sag basin approximately 400 km wide and filled with more than 5 km of sediment. The definitive cause of subsidence of the Basin is still debated, but most authors attribute initial subsidence to thermal contraction after a Proterozoic mantle heating event (Nunn et al., 1984; Ahern and Dikeou, 1989; Catacosinos et al., 1990; Howell and van der Pluijm, 1999). The Basin is bound by the Findlay arch to the southeast, the Kankakee Arch to the southwest, the Wisconsin Arch to the west, and the Canadian Shield to the north (Catacosinos et al., 1991).

Precambrian granites and metamorphic rocks of southern Michigan are divided into 4 basement provinces (Figure 1). Penokean rocks in the north are split by a south-southeast trending gravity anomaly identified as a failed Keweenawan rift (Hinze et al., 1975). Some authors consider this rift an extension of the Illinois Reelfoot Rift (Sleep et al., 1980; Howell and van der Pluijm, 1990), while others suggest it is an arm of the Mid-Continent Rift (Van Schmus and Hinze, 1985; Drahovzal et al., 1992). In this study, we will refer to this underlying rift system as the Mid-Michigan Rift (MMR).

Cambrian rocks are mostly marine quartzose sandstones that record continually

deepening upward cycles with increasing volumes of shale (Figure 2). Carbonates become more dominant higher in section (Catacosinos, 1973). Detailed descriptions of Michigan Basin stratigraphy can be found in Catacosinos (1973), Lilienthal (1978), and Catacosinos et al. (1991).

Ordovician rocks in Michigan are primarily comprised of limestones, dolomites, and shales (Figure 2). More detailed descriptions of these strata can be found in Lilienthal (1978) and Catacosinos et al. (1991). Ash beds (k-bentonites) are used as Ordovician stratigraphic markers across much of the Basin including several key markers in the TBR (Grammer and Harrison, 2013). TBR rocks are primarily fossiliferous limestone.

Three major types of dolomite are recognized in the TBR: a regional dolomite observed in the west and southwest of the Basin (Yoo et al., 2000), a thin cap ferroan dolomite directly underlying the Utica Shale in southern and western Michigan (Taylor and Sibley, 1986), and fracture related reservoir dolomites (Gregg and Sibley, 1984; Taylor and Sibley, 1986; Haefner et al., 1988; Coniglio and Williams-Jones, 1992; Yoo et al., 2000). These dolomites are distinguishable based on $\delta^{18}O$ and $\delta^{13}C$ isotopic signatures, $FeCO_3$ content, texture, and regional occurrence.

Based on petrographic and geochemical evidence Yoo, et al. (2000) believed that the regional dolomite likely formed during early shallow burial. It typically is comprised of fine to medium crystalline (0.03 to 0.5mm), non-ferroan planar dolomite (dolomite textural classification of Sibley and Gregg, 1987) and commonly displays cloudy, inclusion rich cores and limpid, inclusion poor rims (Yoo et al., 2000). The cap dolomite, described by Taylor and Sibley (1986), is comprised of fine crystalline (0.01 to 0.03mm), ferroan, planar crystals and is thought to have formed as a result of dewatering of the overlying Utica Shale. Fracture related dolomites are comprised of medium to coarse crystalline (0.1 to 0.8mm) planar to nonplanar replacive dolomite and coarse to very coarse crystalline (0.5+ cm) void-filling, saddle dolomite cements (Gregg and

Sibley, 1984). Cement lined voids consist of vugs, fractures, and breccias and form reservoirs in TBR oil fields (Gregg and Sibley, 1984; Taylor and Sibley, 1986; Haefner et al., 1988; Hurley and Budros, 1990; Catacosinos et al., 1991; Coniglio and Williams-Jones, 1992; Yoo et al., 2000; Wilson et al., 2001; Grammer and Harrison, 2013 and many others). The Albion-Scipio trend in the Michigan Basin is considered a "type example" for hydrothermal dolomite plays (Davies and Smith, 2006).

Overlying Silurian rocks in the Michigan Basin are described in detail by Lilienthal (1978), Fisher et al. (1988), and Catacosinos et al. (1991). The Silurian Salina group contains thick halite and anhydrite units interbedded with thin carbonate and shale layers (Figure 2). Sylvite in the Salina is present in much of the Basin and economic quantities are present in the Basin center (Catacosinos et al., 1991).

Devonian rocks are comprised of a mix of siliciclastics, carbonates, and evaporites. The Dundee Limestone of the Middle Devonian contains fault and fracture related hydrothermal dolomites, which appear to have origins and fluids similar to TBR hydrothermal reservoirs (Luczaj, 2001; Luczaj et al., 2006). The Mississippian system is primarily comprised of shales with some quartzose sandstone and is characterized by Catacosinos et al. (1991) as terrigenous detritus. Only thin remnants of the Pennsylvanian and Jurassic systems are preserved in the Basin. Descriptions for all rocks in the Basin can be found in Lilienthal (1978), Fisher et al. (1988), and Catacosinos et al. (1991).

Tectonics

Initiation of Michigan Basin subsidence is uncertain, but most authors attribute initial subsidence to a failed rift based on a gravity anomaly identified by Hinze et al. (1975) which divides the Basin into 4 basement provinces (Figure 1) (Hinze et al., 1975; Howell and van der Pluijm, 1999). Howell and van der Pluijm (1999) identified 7 structural 'sequences' from an early

open trough to periods of narrow, tilted, and broad basin subsidence styles that do not directly correlate with the sequence boundaries of Sloss (1963) but appear greatly affected by extra-basinal plate-scale orogenic events.

Reactivation of existing Archean basement faults occurred throughout the Basin's history. Evidence for vertical wrench faults over these structures is noted as high in the section as Mississippian strata (Ells, 1962). Northwest trending strike-slip and *en echelon* features over these basement faults likely provided conduits for hydrothermal fluid flow. These features are common throughout the Basin in strata as shallow as the Devonian Dundee Limestone (Prouty, 1988; Luczaj et al., 2006) and in surrounding areas in correlative units, including the Middle Ordovician in Wisconsin (Luczaj, 2001; Luczaj et al., 2006) Indiana and the Ohio Lima Field (Fara and Keith, 1988; Haefner et al., 1988; Yoo et al., 2000), New York (Smith, 2006), and Ontario (Coniglio et al., 1994; Nurkhanuly, 2012;). During early exploration in the TBR, oil fields were missed because they commonly occur in synclinal sag-feature traps over wrench faults (Hurley and Budros, 1990). With the advent of 3D seismic, these sag features became more easily identified for development (Hurley and Budros, 1990; Davies and Smith, 2006; Sagan and Hart, 2006; Jaiswal et al., 2019).

Thermal History

Present day geothermal gradients of near 20° C/km cannot accurately account for elevated thermal maturities observed in the Michigan Basin. A plethora of evidence exists suggesting higher past temperatures and overburden in the Basin. Reconciling the maturity of organic content with present day temperatures and depths provides the basis for discussion. To obtain organic maturity of shallow bituminous Pennsylvanian coals (R_o 0.54 to 0.60; 2.6 TAI equivalent), an additional 2 km of overburden at a geothermal gradient of 25° C/km is required (Moyer 1982; Cercone, 1984). Moyer (1982) using the coloration of spores determined the

entirety of the Late Mississippian Michigan Formation was heated enough to produce oil (TAI 2 to 3). At present burial depths and current temperature gradients, at least 1.6 km of additional overburden is needed to reach oil generating temperatures in the Michigan Formation. Everham (2004) studied vitrinite reflectance in several deep boreholes in south-central Michigan. Slopes drawn through vitrinite reflectance values show a significantly higher heat flow and geothermal gradient in pre-Silurian strata when compared to values for post-Devonian strata in the Basin (Everham, 2004).

Burial models based on organic maturity data lend further support for elevated geothermal gradients and additional overburden. Cercone (1984) used Lopatin modeling to match thermal maturity indicators from Moyer (1982) and suggested additional overburden (up to 1 km) and higher past geothermal gradients (35 to 45° C/km). Vugrinovich (1988) utilized shale decompaction curves to estimate eroded sediment thickness and subsequent Lopatin modeling to determine paleogeothermal gradients. His findings suggest up to 850 m of sediment has been removed from the Basin and past gradients were on the order of 45 to 65° C/km to match thermal alteration of organic matter in Precambrian through Mississippian sediments.

Geochemical and petrological data provide additional evidence for Michigan Basin thermal history. Temperatures for authigenic illite formation in the Ordovician St. Peter Sandstone require a paleo-geothermal gradient twice that of the current gradient at present depths (Girard and Barnes, 1995). Fluid inclusion temperatures in the same study indicate post entrapment heating of inclusions to greater than 150° C (Girard and Barnes, 1995). Fluid inclusion temperatures of saddle dolomites in the Devonian Dundee Limestone suggest dolomite precipitation occurred at 120 to 150° C, which is considerably higher than present day temperatures of 40 to 45° C at a depth of ~1.3 km (Luczaj et al., 2006). Authigenic minerals in the Upper Paleozoic Marshall and Dundee Formations indicate paleo-temperatures above what

could be produced by current burial depths (Cox, 2015). Cox (2015) suggested heat from episodic hydrothermal activity as the most likely source of heat for the formation of these minerals.

Based on the above evidence, a combination of an elevated geothermal gradient (at least 34° C/km and up to 56° C/km) and additional overburden (850 to 2000 m) must have existed in the Michigan Basin in the past. The cause of elevated geothermal gradients in the Basin is still uncertain. Some authors cite additional overburden acting as a thermal blanket during early Basin history (Cercone, 1984; Luczaj et al., 2006) while others favor heating by brief thermal events, potentially caused by orogenic episodes outside the Basin (Girard and Barnes, 1995; Howell and van der Pluijm, 1999; Cox, 2015).

Fault Fracture Oil Fields

Fault-fracture dolomite hosted petroleum fields are of considerable interest, both in the Michigan Basin, as well as around the world. Their similarity to Mississippi Valley-Type (MVT) base metal deposits in terms of temperatures of formation, mineral assemblages, and structural features is well documented (Ells, 1962; McNutt et al., 1987; Haefner et al., 1988; Hurley and Budros, 1990; Budai and Wilson, 1991; Allan and Wiggins, 1993; Wilson et al., 2001; Davies and Smith, 2006; Grammer and Harrison, 2013; Jaiswal et al., 2019; and many others).

Work on TBR fault-fracture dolomite reservoirs extends from the Michigan Basin into surrounding areas including New York (Smith, 2006), Ontario, (Coniglio and Williams-Jones, 1992; Coniglio et al., 1994), Indiana (Fara and Keith, 1988; Yoo et al., 2000), Ohio (Haefner et al., 1988), and Wisconsin (Luczaj, 2001; Luczaj 2006). Reservoir dolomites in the TBR occur locally near brittle failure surfaces and grade into non-productive host limestone within a few tens of meters (Hurley and Budros, 1990). Brittle failure surfaces exhibit the main control over dolomite reservoir distribution, but Grammer and Harrison (2013) show evidence that

depositional facies within a well-defined stratigraphic framework influenced preferential dolomitization away from active fault zones (Figure 3).

Considerable work has been done on the prolific Albion-Scipio trend (Ells, 1962; Hurley and Budros, 1990; Allan and Wiggins, 1993; Budai and Wilson, 1991; Wilson et al., 2001) but smaller TBR fields in southern Michigan remain largely unstudied, and field-to-field comparisons are lacking. This study systematically compares several fields of various sizes across the south-central Basin area (Figure 4).

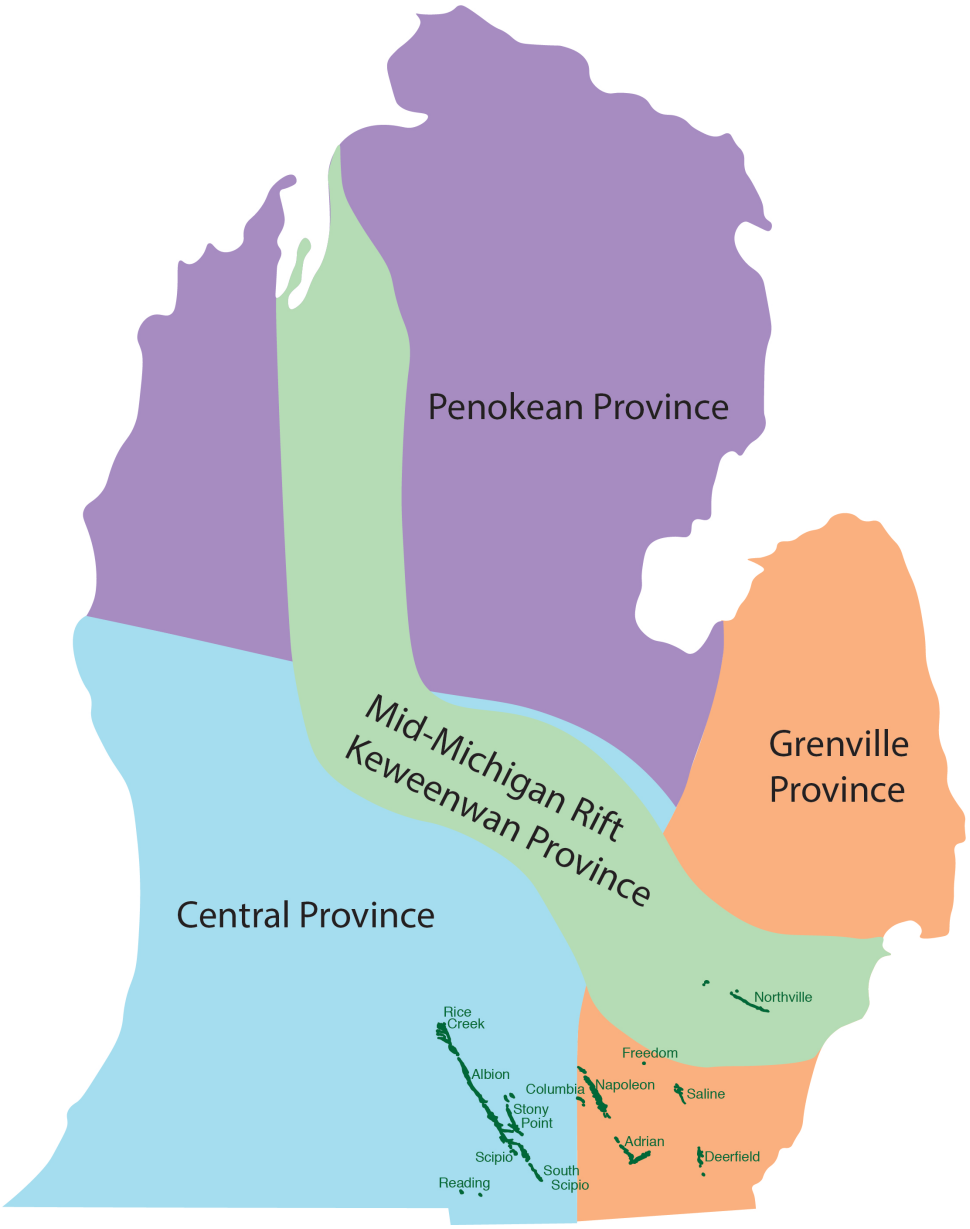

Figure 1: Basement Provinces of Southern Michigan. Basement rocks underlying the southern Michigan peninsula are comprised of four basement provinces. Middle Ordovician Trenton and Black River oil fields of south-central Michigan are displayed. After Hinze et al., 1975.

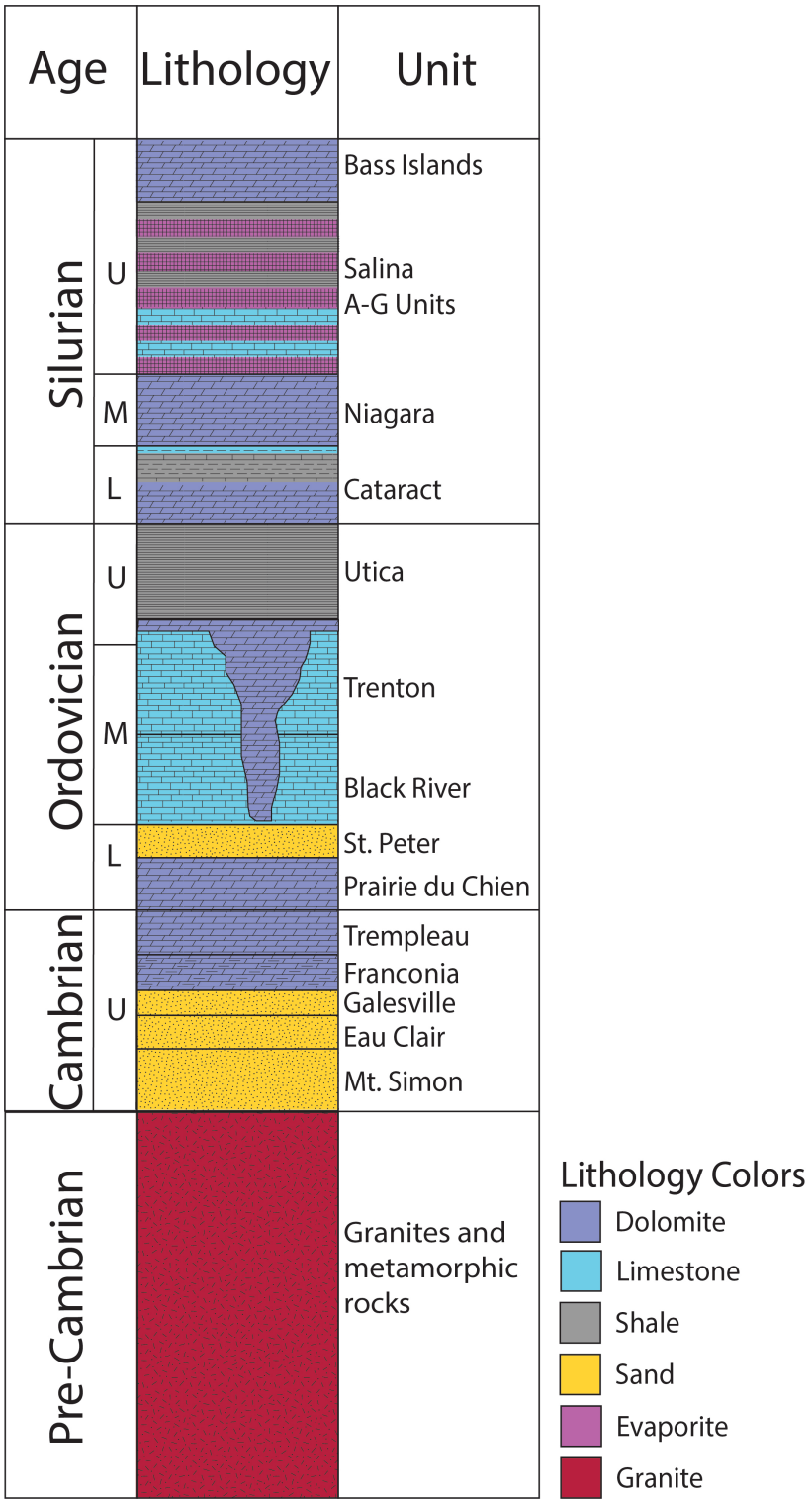

Figure 2: Stratigraphic Column. Stratigraphic column showing lower Paleozoic units in the south-central Michigan Basin.

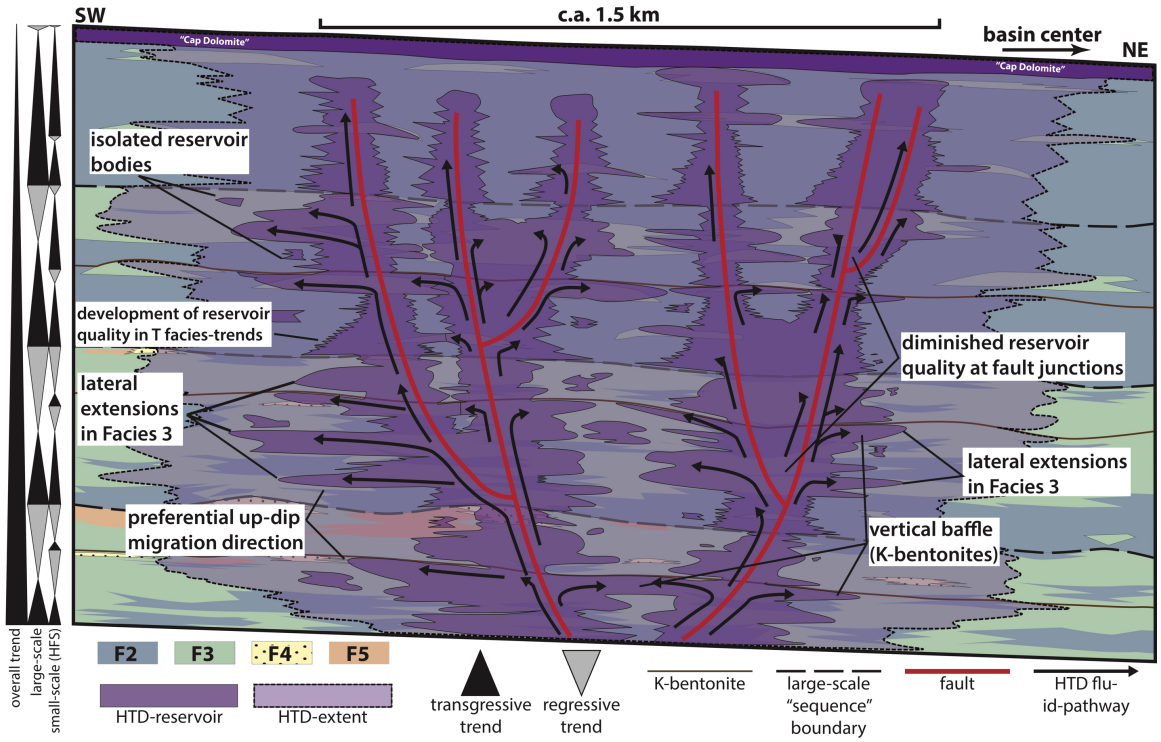

Figure 3: Dolomitization Model for Trenton and Black River Oil Fields. Proposed model of dolomitization for Trenton-Black River dolomite reservoirs. From Grammer and Harrison (2013).

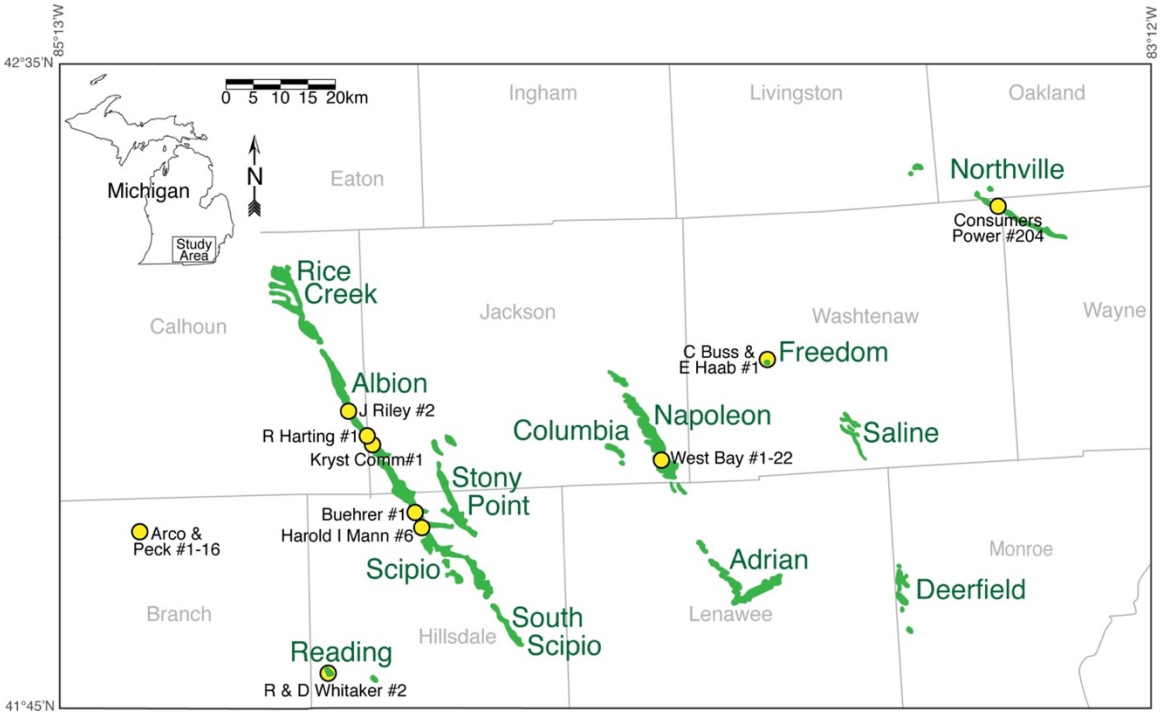

Figure 4: Map of Study Area. Productive fault-fracture Ordovician trends of the south-central Michigan Basin are shown in green. Locations of cores used in this study are highlighted with yellow circles.

CHAPTER III

METHODS

Thirty polished thin section billets cut from 6 cores housed at the University of Michigan were collected by Jay M. Gregg in 1986. An additional 8 billets were cut from samples obtained from 4 cores accessed by G. Michael Grammer and the author at the Michigan Geological Repository for Research and Education (MGRRE) in 2017. Additional archived samples were examined from the research collection of Jay M. Gregg (see Gregg, 1982 and Gregg and Sibley, 1984). A total of 35 polished thin sections were prepared from these samples and studied. Petrography was conducted on an Olympus BX51 microscope. Cathodoluminescence (CL) photomicrographs of each thin section were taken using a CITL MK5-1 cold cathode optical cathodoluminescence system mounted on an Olympus BX51 microscope. Photomicrographs of each thin section were taken using a "Q-Color 3" cooled (low light) 5-megapixel digital microscope camera.

A total of 14 polished thick sections selected from among the above-mentioned samples were made for fluid inclusion studies. Fluid inclusion microthermometry was performed using a Linkam THMS600 microscope stage mounted on an Olympus BX41 microscope. Individual fluid inclusions were analyzed multiple times for homogenization (T_h), eutectic (T_e), and last ice melt (T_m) temperatures. T_m temperatures were converted to equivalent weight percent NaCl (wt. % NaCl) using the equation of Bodnar and Vitnyk (1994). No pressure corrections were made on fluid inclusions because depth of burial at the time of formation is uncertain. Error for T_h is ±1° C

and ±0.3° C for T_m. Inclusions were identified as primary, secondary, or pseudo-secondary as described by Goldstein and Reynolds (1994). Hydrocarbon inclusions were identified using ultraviolent epifluorescence prior to microthermometry.

Sixty-five samples of host limestone, dolomite and calcite cements, and calcite skeletal fragments were drilled from the original thin section billets for carbon and oxygen isotope analysis. Carbon and oxygen isotope analyses for all samples were run at the Stable Isotope Laboratory at the University of Miami's Rosenstiel School of Marine and Atmospheric Science. Errors for $\delta^{18}O$ and $\delta^{13}C$ relative to the VPDB standard are ±0.05‰. A total of 10 samples of dolomite and calcite cements were analyzed for $^{87}Sr/^{86}Sr$ at the University of Kansas Radiogenic Isotope Laboratory. Errors for $^{87}Sr/^{86}Sr$ are ±0.000014 within a 95% confidence interval.

CHAPTER IV

RESULTS

Optical Petrography

Host limestones are comprised of fossiliferous wackestone to packstone. Fossil fragments include crinoids, brachiopods, thin-walled bivalves, and rare rugose coral fragments. Fine grained (<0.05 mm) nonplanar dolomite crystals appear to replace original lime mud matrix. Host limestone appears to have little to no porosity in core, billets, or thin section. Rare centimeter scale voids are typically lined by 0.5 to 5 mm saddle dolomite cement crystals. Blocky calcite and anhydrite cements occasionally fill remaining void space.

Dolomite matrix replacing limestone typically displays nonplanar to planar-e texture. Dolomite crystals <0.05 mm appear darker brown in plane light (PL) and are nonplanar while larger crystals tend to display planar-s to planar-e texture and commonly show ‘cloudy’, inclusion rich cores and limpid, inclusion poor rims. Replacive dolomite crystals are medium brown to pale yellow in PL and are easily distinguishable from more limpid coarse dolomite cements in PL and cross-polarized light (XPL). Replacive dolomite has little to no intercrystal porosity. Porosity in replacive dolomites exists as centimeter-scale voids and, less frequently, fractures, which are typically lined by carbonate, sulfide, and sulfate cements. Figure 5 displays the general paragenesis for TBR oil fields.

Dolomite cements consist of white, void-filling saddle dolomite crystals ranging in size from 0.25 mm to 2 cm or more. In open void space they are planar-e. When cements have intergrown to fill all void space they form a nonplanar mosaic. Curvature on saddle dolomite crystal faces are observed in centimeter-sized crystals in core and in thin section (Figures 6 and 7). Cements commonly have cloudy, fluid inclusion rich cores and limpid, fluid inclusion poor rims. Distinctive sweeping extinction is observed in XPL in most thin sections (Figures 6 and 7). Late calcite cements are very coarse, centimeter-scale, blocky crystalline. They fill open space in Northville oil field and Branch County samples and are less inclusion rich than dolomite cements (Figures 6 and 8). Infrequently, anhydrite, sphalerite, and pyrite crystals are observed filling open space and paragenetically follow calcite cement. Hydrothermal breccias frequently host dolomite clasts 'floating' in dolomite cement, and vertical and horizontal fracture cement fill, on the millimeter to centimeter scale, are observed in both core and thin section (these features also were observed by Coniglio et al., 1994 and Grammer and Harrison, 2013). Vugs up to 10 cm wide, in the largest dimension, are observed in core and contain void lining and void filling saddle dolomite crystals 1 mm to 1 cm in diameter. Cement-filled fractures of 1 cm or less appear non-porous in core, but typically reveal intercrystal porosity (100 μm to 0.5 mm) between cement crystals (~0.5 mm diameter) in thin section, usually in void or channel 'centers' (Figures 7, 9, and 10). Petroleum fluid inclusions in cements were identified under UV light in all samples except for those from the Branch County core. Small amounts of bitumen are observed in most samples in core and thin section within cements and coating cements lining voids. Petroleum staining and even solid bitumen is observed coating ~1 cm saddle dolomite crystals on ends of core slabs where open pore space existed.

Cathodoluminescence Petrography

Cathodoluminescence (CL) responses may develop as a distinctive growth stratigraphy in carbonate cement crystals based on compositional zoning inherited from changing composition of cement precipitating fluids. Band patterns are used to correlate CL stratigraphy among samples and thus, potentially identify common fluid histories among samples (Voss et al., 1980).

Host Limestone fossil fragments display yellow CL (Figure 11). Matrix replacement dolomites <0.05 mm display uniform moderate red CL (Figures 10 and 12). Larger replacive dolomites (>0.05 mm in diameter) commonly display a 2 color CL pattern: inclusion rich cores (25+ μm diameter) display bright red CL response and are terminated by moderate to dull CL inclusion poor rims (.025+ mm wide) (Figures 7B, 9B, and 10B).

Dolomite cements typically display moderate, low, or non-CL response as distinctive growth zones or bands. In samples from several oil fields including Reading, Scipio, and Freedom, dolomite cements display multiple distinct CL bands (Figures 9B, 10B, and 12B). Samples from the Branch County core and the Napoleon field (Figures 6B and 13B) display a single CL band. Dolomite cements from the Albion (Figure 7B) and Northville fields (Figure 8B) display 2 CL bands. Samples from the Northville field also contain bright yellow CL void-filling blocky calcite cement. Dolomite cements occasionally display bright blue 'speckled' CL spots ~0.05 mm in size (Figure 12B), which Budai and Wilson (1991) identify as authigenic K-feldspar. Table 1 summarizes CL banding and Figures 6 through 13 display detailed descriptions of banding in each oil field.

Fluid Inclusion Microthermometry

Small imperfections during crystal growth form void spaces that capture aqueous fluid present during crystal formation (Bodner and Samson, 2003). These fluid inclusions can contain vapor, brine, oil, gases, and solid daughter crystals in any combination. Fluid inclusions in this study were grouped into assemblages. An assemblage is a group of fluid inclusions that were formed, in theory, by the same fluid at the same time (Goldstein, 2003). Grouping individual inclusions into assemblages may allow for greater statistical certainty of homogenization (T_h) and last ice melt (T_m) measurements and prevents bias of data toward easily measured inclusions. First ice melt temperatures are interpreted as eutectic temperatures (T_e). Measured inclusions used in this study contain two or more phases: liquid, vapor, and less commonly, solid daughter halite crystals. A summary of values for fluid inclusion measurements by oil field is given in Table 2 and all fluid inclusion measurements are included in Appendix I. Values are uncorrected for pressure. Figure 14 displays examples of common fluid inclusion types in this study, and Figure 15 is an example of hydrocarbon inclusions from the Albion oil field.

Fluid inclusions measured in dolomite cement in this study are most frequently primary (Figure 14A and 15). Inclusions measured in calcite cements in the Northville field are interpreted as secondary where observed in healed fracture planes (Figure 14B). No obvious primary fluid inclusions were measured in Northville field calcite cements. Fluids observed in this study fall into two distinct temperature clusters (Figures 16 and 17). A warm fluid with T_h ranging from ~110° to 175° C, and a hot fluid ranging from ~180° to 250+° C. Salinities in the warm fluid range from 16-39 weight % NaCl equivalent, while the hot fluid salinity ranges from 22 to 49 weight % NaCl equivalent. Hydrocarbon inclusions appear to be largely secondary although, primary petroleum inclusions were observed less frequently. Only T_h measurements were obtained for hydrocarbon inclusions. Hydrocarbons are observed as late-stage fluid

inclusions in all producing oil fields in this study. Hydrocarbon inclusions were not observed in the non-productive Branch County well.

Eutectic temperatures (T_e) as low as -89° C were observed for many dolomite and calcite fluid inclusions and most commonly clustered around -64° C. This is far lower than the eutectic temperature (T_e) of -21.2° C for a pure NaCl brine (Bodnar, 2003). Eutectic temperatures below that of a pure NaCl system are typically interpreted as indicating divalent cations other than sodium are present in fluids (Bodnar, 2003). The eutectic temperature of the H_2O-NaCl-CaCl system is approximately -52° C and melting is frequently recognizable between -40° C and -50° C (Bodnar, 2003). Hydrohalite formed infrequently during freezing and melted around -3.5° C. Hydrohalite was identified by its cloudy appearance when compared to more limpid water ice crystals and its final melting temperature close to 0° C.

Isotope Geochemistry

Table 3 contains $\delta^{18}O$ and $\delta^{13}C$ data measured in this study and Figure 18A displays $\delta^{18}O$ vs $\delta^{13}C$ isotope values. Host limestone values of $\delta^{18}O$ vs $\delta^{13}C$ correspond to published values for Middle to Upper Ordovician seawater (Qing and Veizer, 1994). Replacive matrix dolomite and dolomite cement $\delta^{18}O$ values range from -10.5‰ to -6.5‰, and $\delta^{13}C$ values range from -1.2‰ to 1.6‰. Replacive dolomite, dolomite cement, and calcite cement values correspond to those of previous studies for TBR hydrothermal dolomites (Taylor and Sibley, 1986; Haefner et al., 1988; Budai and Wilson, 1991; Allan and Wiggins, 1993; Coniglio et al., 1994; Yoo et al., 2000; Grammer and Harrison, 2013).

Clustered trends of $\delta^{18}O$ and $\delta^{13}C$ by field are recognized (Figure 18B). Branch County core dolomite values are tightly clustered with less depleted $\delta^{18}O$ and more depleted $\delta^{13}C$ than other fields. Reading field values for $\delta^{18}O$ span the whole study grouping, with a slightly tighter

range of positive $\delta^{13}C$ values. Reading field replacive dolomites all fall below -9‰ $\delta^{18}O_{VPDB}$ and dolomite cements are above -9‰ $\delta^{18}O_{VPDB}$. Albion field values form a tight cluster more depleted in $\delta^{13}C$ compared to other fields. Albion field cements tend to be more depleted in $\delta^{18}O$ than their replacive dolomite values. One outlier replacive dolomite for the field is more enriched in $\delta^{18}O$ and $\delta^{13}C$ than other values in the study and plots in the equilibrium field for Middle-Upper Ordovician seawater (Figure18A). Scipio field dolomites form a tight cluster of values centered among the other fields. Napoleon field values are more broadly scattered and display more positive $\delta^{13}C$ values than Scipio or Albion samples with similar $\delta^{18}O$ values. Freedom field dolomites have a broader range of $\delta^{13}C$ than most other fields and its $\delta^{18}O$ values are centered among the other fields. Replacive dolomites in Northville field all display positive $\delta^{13}C$ values and are centered among other field $\delta^{18}O$ values. Northville dolomite cements are the only productive field that display negative $\delta^{13}C$ values.

Calcite cement values for the Albion and Northville oil fields are depleted in both $\delta^{18}O$ and $\delta^{13}C$ compared to their respective dolomite values, and form separate clusters distinct from dolomite. Calcite in Freedom field is more negative in $\delta^{13}C$, but in the mid-range for $\delta^{18}O$ dolomite values in that field. Calcite cement in the Branch County core is less depleted in $\delta^{18}O$ and $\delta^{13}C$ compared to dolomites in the field.

Values of $^{87}Sr/^{86}Sr$ for most dolomite cements in this study fall from 0.70827 to 0.70944 and are given in Table 4. Values for dolomite and calcite cements in Northville field were much higher than other measurements ranging from 0.71099 to 0.71088. Figure 19 displays $^{87}Sr/^{86}Sr$ values plotted on the Phanerozoic seawater curve (Veizer et al., 1999) and Figure 20 displays $^{87}Sr/^{86}Sr$ values plotted against $\delta^{18}O$.

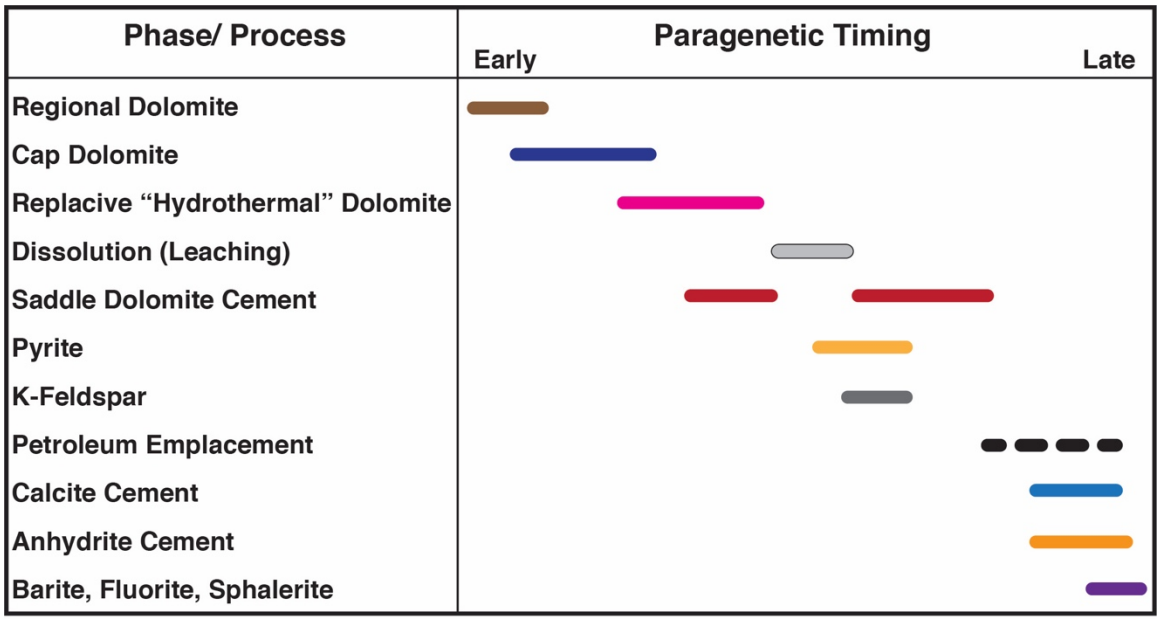

Figure 5. Generalized Paragenesis of Middle Ordovician Oil Fields. Generalized paragenesis for Trenton-Black river dolomite reservoirs of the south-central Michigan Basin. After Budai and Wilson (1991).

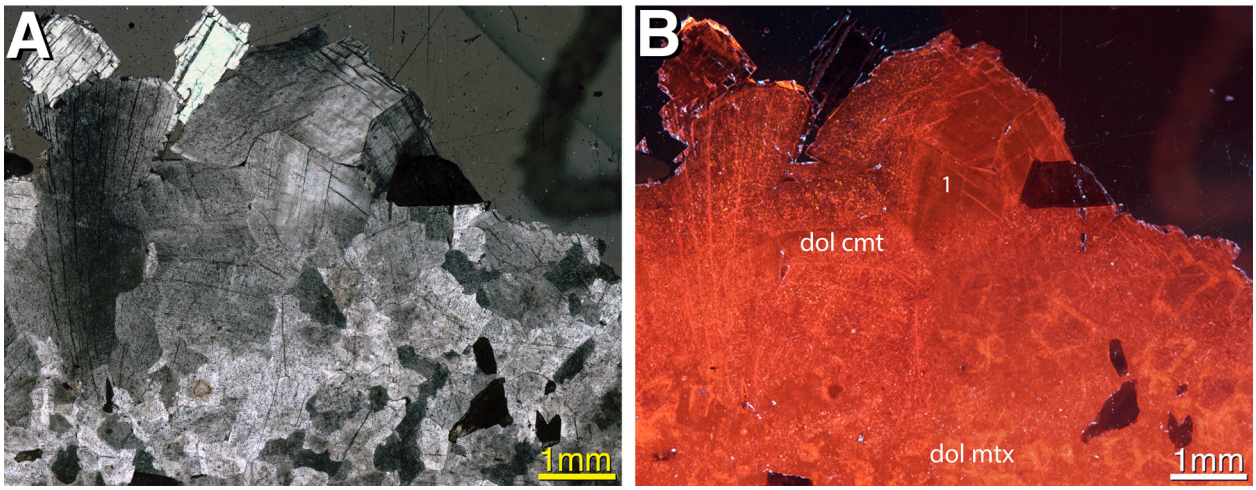

Figure 6: Branch County Core Cements in XPL (A) and CL (B). Matrix dolomite (dol mtx) (200 µm to 1mm) is nonplanar and exhibits moderate CL. 1) Void filling dolomite cements (dol cmt) (1 to 3 mm) are inclusion-rich with moderate CL.

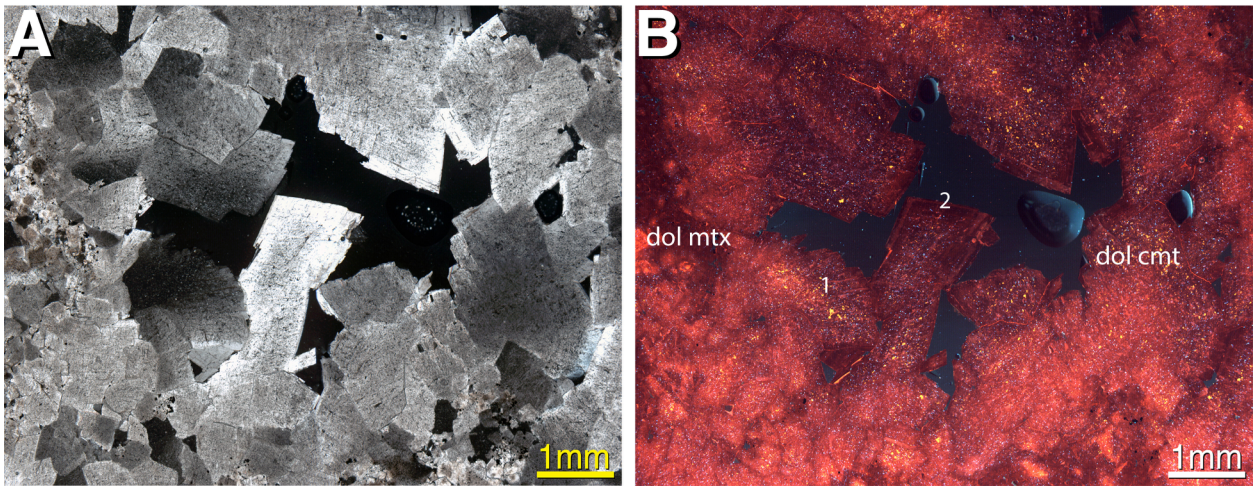

Figure 7: Albion Field Cements in XPL (A) and CL (B). 1) Saddle dolomites (dol cmt) (1 to 5mm) have bright CL, inclusion-rich cores with bright yellow-orange 'speckles' and gradually grade to dull-moderate CL near edges with a sharp contact to 2) a thin (100µm) dull CL, inclusion-poor band.

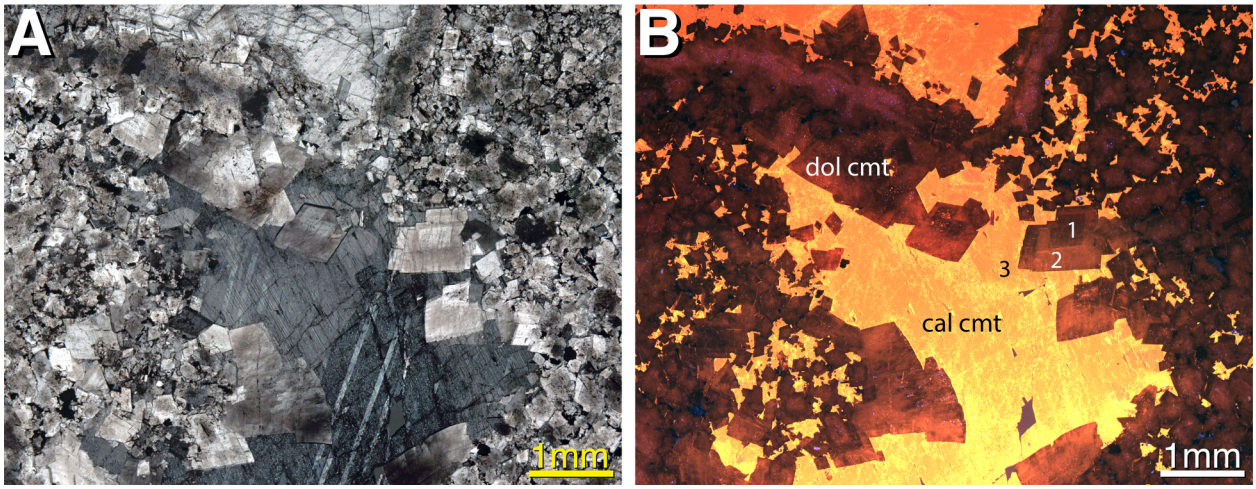

Figure 8: Northville Field Cements in XPL (A) and CL (B). Dolomite cements (dol cmt) have 1) inclusion-rich moderate to dull CL cores (250 µm) and 2) a moderate CL outer band (250 µm). 3) Late stage, blocky, void-filling calcite cement (cal cmt) is bright yellow CL.

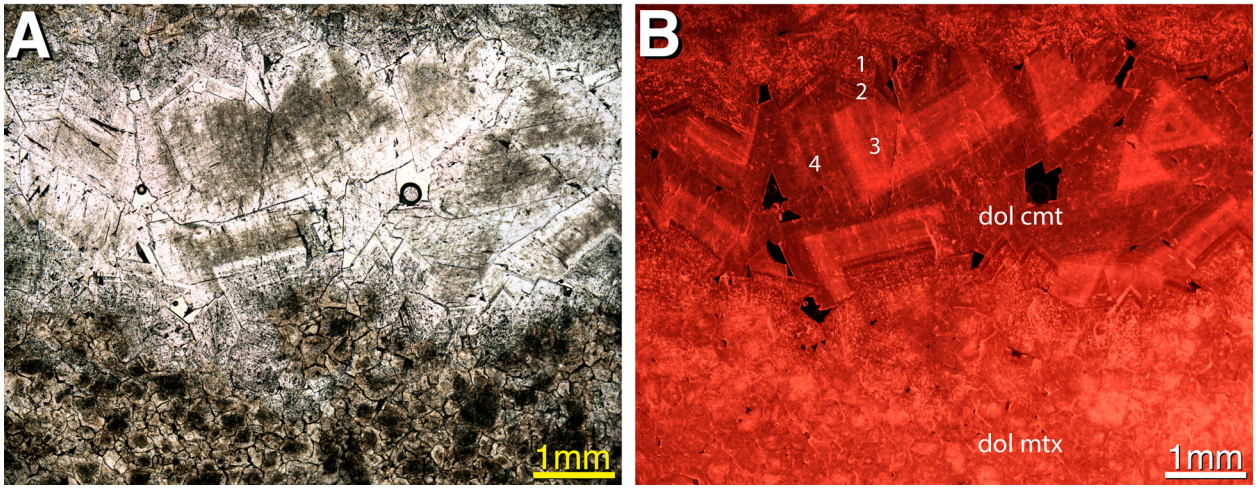

Figure 9: Reading Field Cements in PL (A) and CL (B). Void lining saddle dolomites (dol cmt) (300 µm to 1mm) have 1) inclusion-rich bright CL cores that grade to moderate CL prior to 2) a pair of thin dull-moderate CL couplets. Void filling dolomites have 3) large (100 to 500 µm) inclusion-rich bright CL cores followed by 4) a thick (250 µm to 1mm) inclusion-poor rim of dull CL.

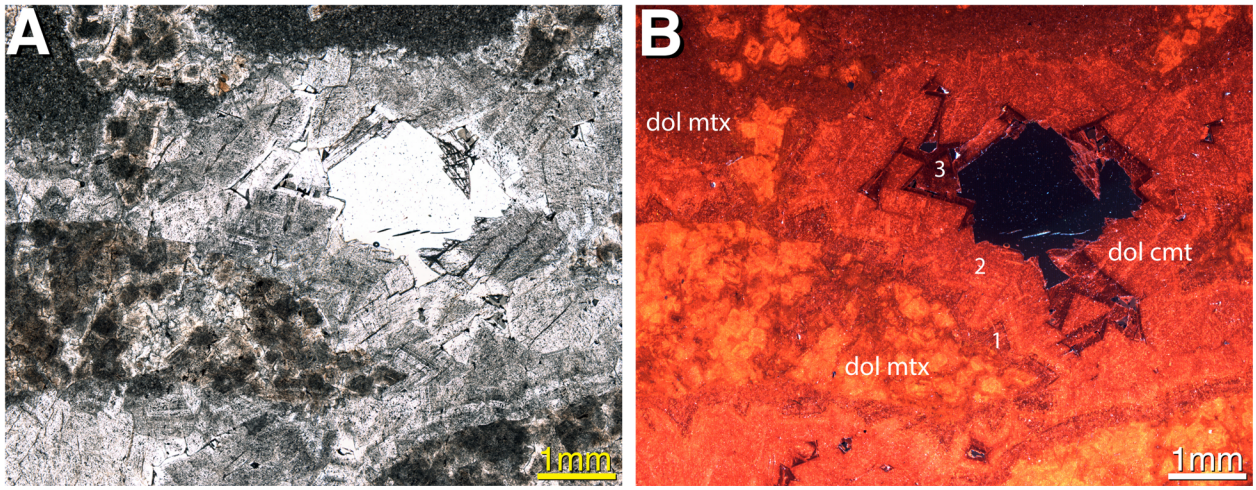

Figure 10: Scipio Field Cements in PL (A) and CL (B). Void lining dolomite cements (dol cmt) (150 to 250 µm) capping replacive dolomite (dol mtx) (250 µm) have 1) dull-moderate CL followed by 2) moderate-bright CL, inclusion-rich cement band (500 µm to 1 mm) then a sharp contact to 3) a wide, inclusion-poor, dull CL band (100 to 300 µm).

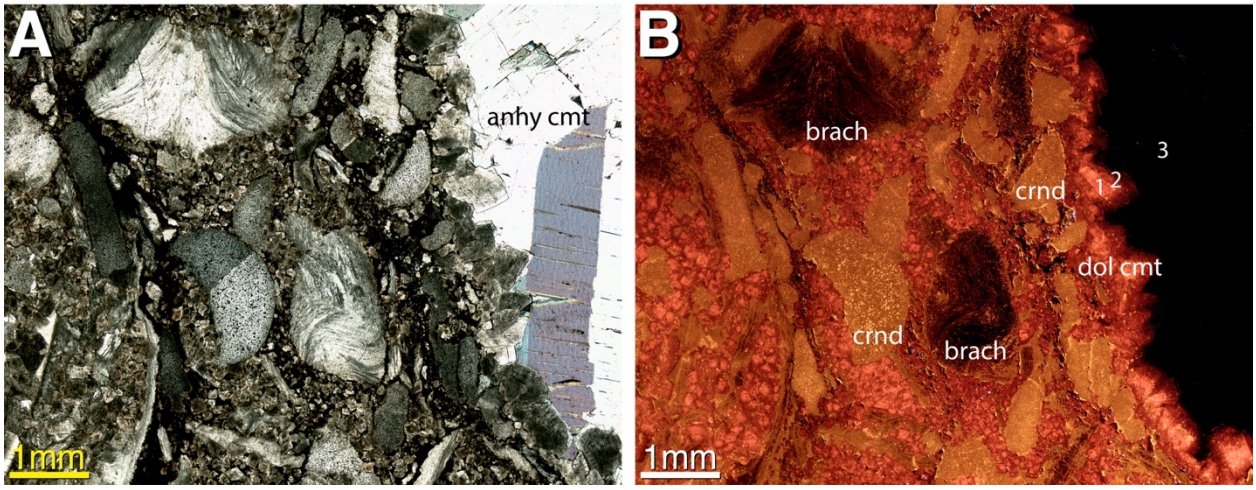

Figure 11: Host limestone from Freedom field in XPL (A) and CL (B). Fine crystalline (10 to 20 µm) planar-e to planar-s matrix dolomites display cloudy, inclusion-rich cores and clearer, inclusion-poor rims. In CL, cores are bright orange with moderate red-orange rims. Crinoid (crnd) and bivalve skeletal fragments are calcite and display moderate to bright yellow CL. Brachiopod skeletal fragments (brach) are non-CL. Void lining dolomite (20 to 50 µm) cements (dol cmt) have 1) bright CL, inclusion-rich cores and 2) thin inclusion poor, moderate CL rims. 3) Non-CL anhydrite cement (anhy cmt) fills void.

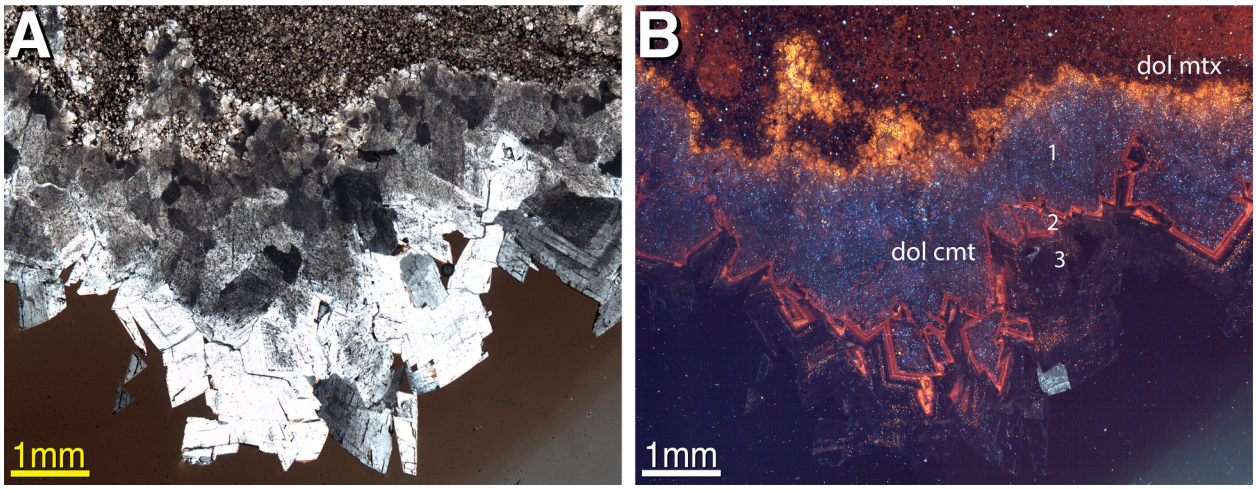

Figure 12: Freedom Field Cements in XPL (A) and CL (B). 1) Inner dolomite cements (dol cmt) (100 to 500µm) are planar-s near matrix and planar-e toward voids. They are inclusion-rich with very dull CL with common bright blue CL speckles. Budai and Wilson (1991) identify these blue speckles as potassium feldspar replacing dolomite. The edge of these crystals shows 2) a thin (50 to 100µm) bright-dull-bright CL banding. This is followed by 3) a final thick band (300µm to 3mm) of coarse saddle dolomite (1mm) that is inclusion-poor and non-CL.

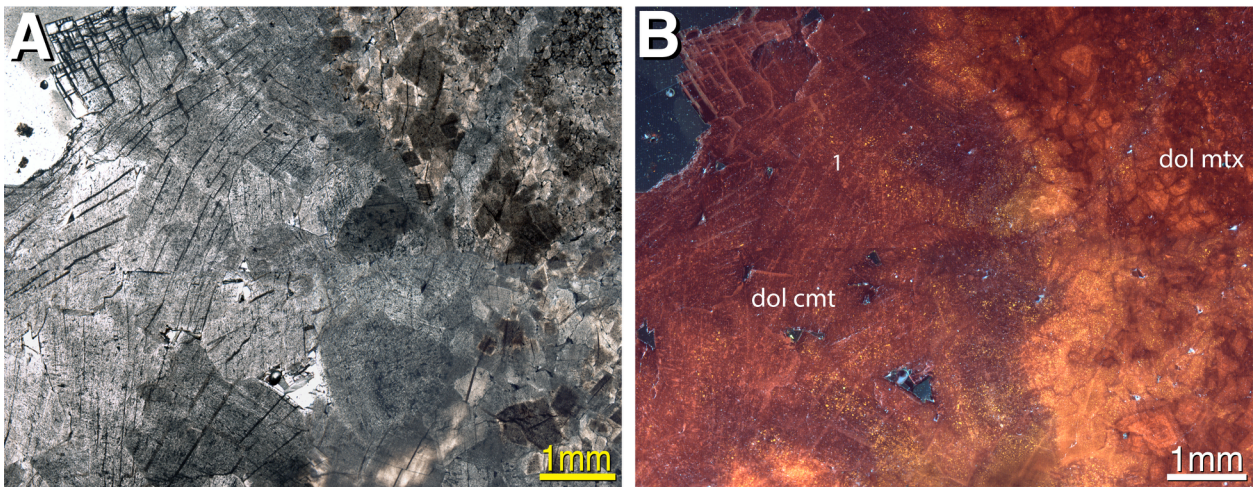

Figure 13: Napoleon Field Cements in PL (A) and CL (B). Medium crystalline (100 to 500µm) matrix dolomites (dol mtx) gradually transition into dolomite cements (dol cmt) and appear planar-s in cross polarized light and more planar in CL light with bright CL inclusion-rich cores and moderate to dull CL inclusion-poor rims. 1) Coarse dolomite cements (5+mm) are non-planar, uniform moderate to dull red CL with bright yellow-orange 'speckles' and rare curved saddle edges where voids are not completely cemented.

Table 1: Summary of Cathodoluminescence Patterns by Oil Field. Band numerals correspond to numerals and more detailed descriptions by field in Figures 6 through 13.

Field	Lithology	Matrix CL	Cement CL Bands
Freedom	Host Limestone	Bright orange cores with moderate red rims	1) bright dolomite; 2) moderate dolomite; 3) Non-CL anhydrite
Branch County Core	Dolomite	Uniform moderate orange	1) Uniform moderate orange
Reading	Dolomite	Bright orange cores with moderate red rims	1) moderate; 2) two dull-moderate couplets; 3) bright; 4) moderate
Scipio	Dolomite	Bright orange cores with moderate red rims	1) dull moderate; 2) moderate; 3) dull
Albion	Dolomite	Moderate to dull	1) bright grading to dull-moderate with bright yellow speckles; 2) dull
Napoleon	Dolomite	Moderate or bright cores and moderate rims	1) Uniform moderate to dull with bright yellow speckles
Freedom	Dolomite	Moderate to dull	1) Very dull with bright blue speckles; 2) bright-dull-bright triple band; 3) very dull to non-CL
Northville	Dolomite and Calcite	Dull	1) Dull dolomite; 2) moderate dolomite; 3) bright yellow calcite

Table 2: Fluid inclusion data by field. Fluid inclusion measurements of T_h, % wt. NaCl, and T_e when recorded. Fluids are grouped into 2 categories: a warm fluid group (<180°C), and a hot fluid group (>180°C). Both fluid groups may not present in all fields. No pressure corrections have been made on these measurements. T_m values are converted to wt. % NaCl equivalent using the equation of Bodnar and Vitnyk (1994).

Field	Warm T_h °C	Warm T_h Avg °C	Warm % wt. NaCl	Warm % wt. NaCl Avg	Hot T_h °C	Hot T_h Avg °C	Hot % wt. NaCl	Hot % wt. NaCl Avg	T_e °C
Branch Cty Core	79 to 130	124	16.0 to 27.2	24.8	-	-	-	-	-63.8
Reading	113 to 176	133	16.3 to 25.0	20.0	-	-	-	-	-
Scipio	124 to 168	148	26.8 to 32.0	29.3	-	-	-	-	-65 to -57
Albion	110 to 148	122	24.3 to 31.0	27.7	200 to 240	218	25.4 to 35.7	28.6	-
Napoleon	95 to 169	128	27.6 to 38.5	31.1	203 to 213	208	36.3	36.3	-89 to -63
Freedom	91 to 155	117	30.0 to 35.1	32.2	183	183	31.2	31.2	-50
Northville	-	-	-	-	163 to 258	219	15.0 to 49.4	28.3	-112 to -104

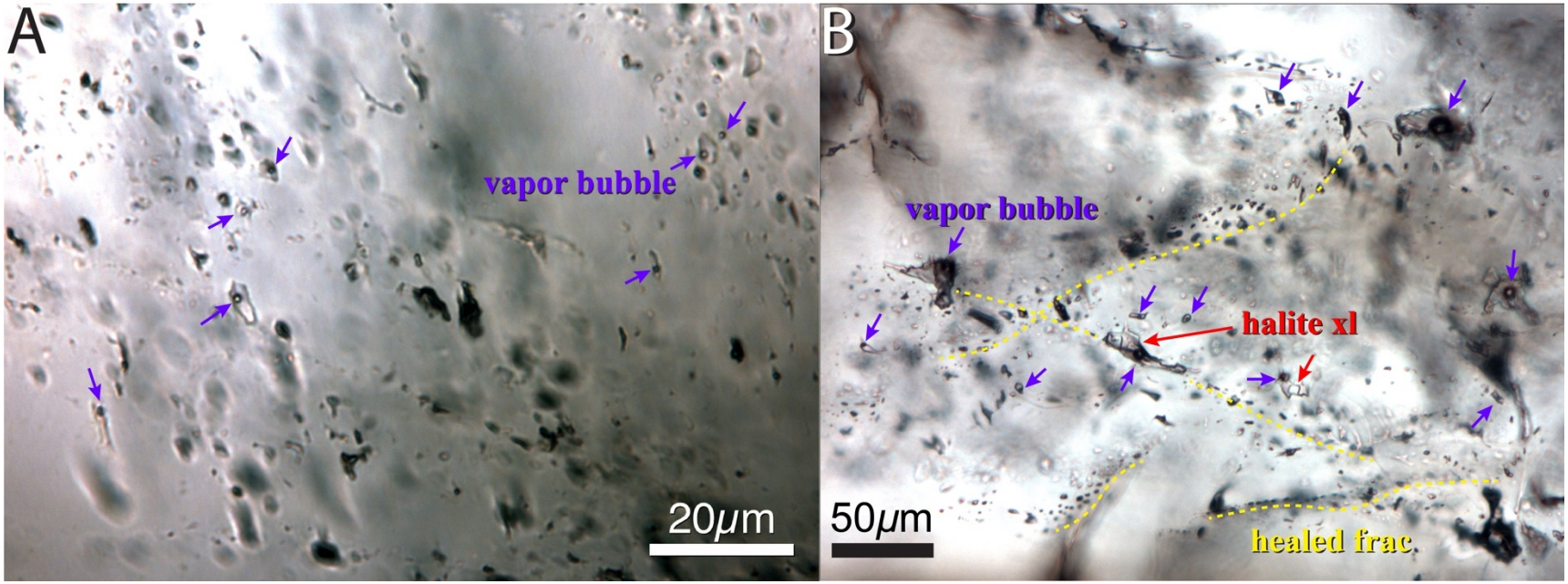

Figure 14: Examples of Fluid Inclusions. A) Two-phase fluid inclusions, aqueous and vapor, in dolomite cement from the Albion oil field in PL. Most inclusions are less than 10 μm in diameter. This type and size of inclusion are the most common in this study. Vapor bubbles are noted by purple arrows. B) Examples of inclusions from Northville oil field calcite cements in PL. Inclusions can be two-phase, aqueous and vapor, or three-phase, aqueous, vapor and daughter halite crystal. Halite daughter crystals are noted by red arrows. Inclusions in calcite cements (up to 40 μm in diameter) are typically larger than those seen in dolomite cements in this study. Inclusions in Northville oil field calcite cements are commonly identified as secondary inclusions in healed fractures. Fracture traces indicated by yellow dashed lines.

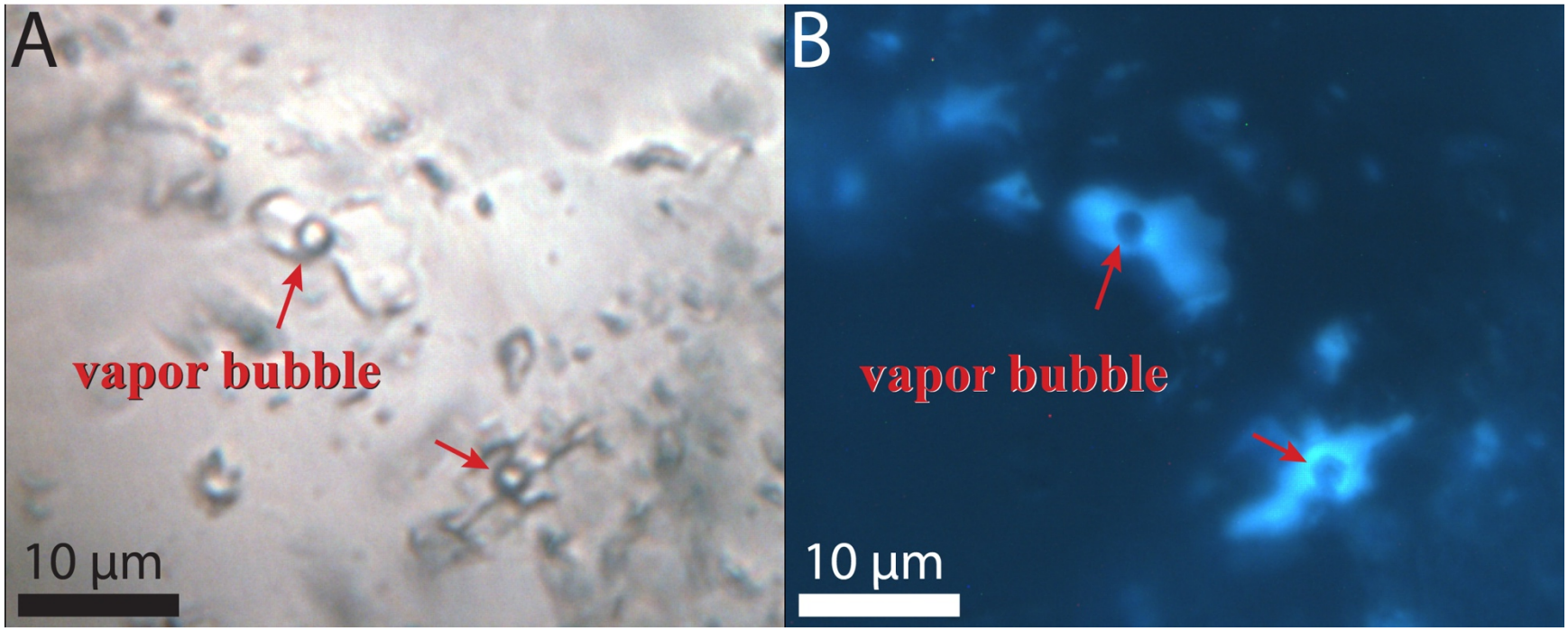

Figure 15: Examples of Petroleum Fluid Inclusions. A) Two-phase fluid inclusions, aqueous and vapor, from dolomite cement in Albion oil field in PL. Vapor bubbles are noted by red arrows. B) The same field of view in fluorescent light (FL). Aqueous portions of the inclusion fluoresce bright pale blue indicating the inclusion contains petroleum fluids. Vapor bubbles appear as dark circles.

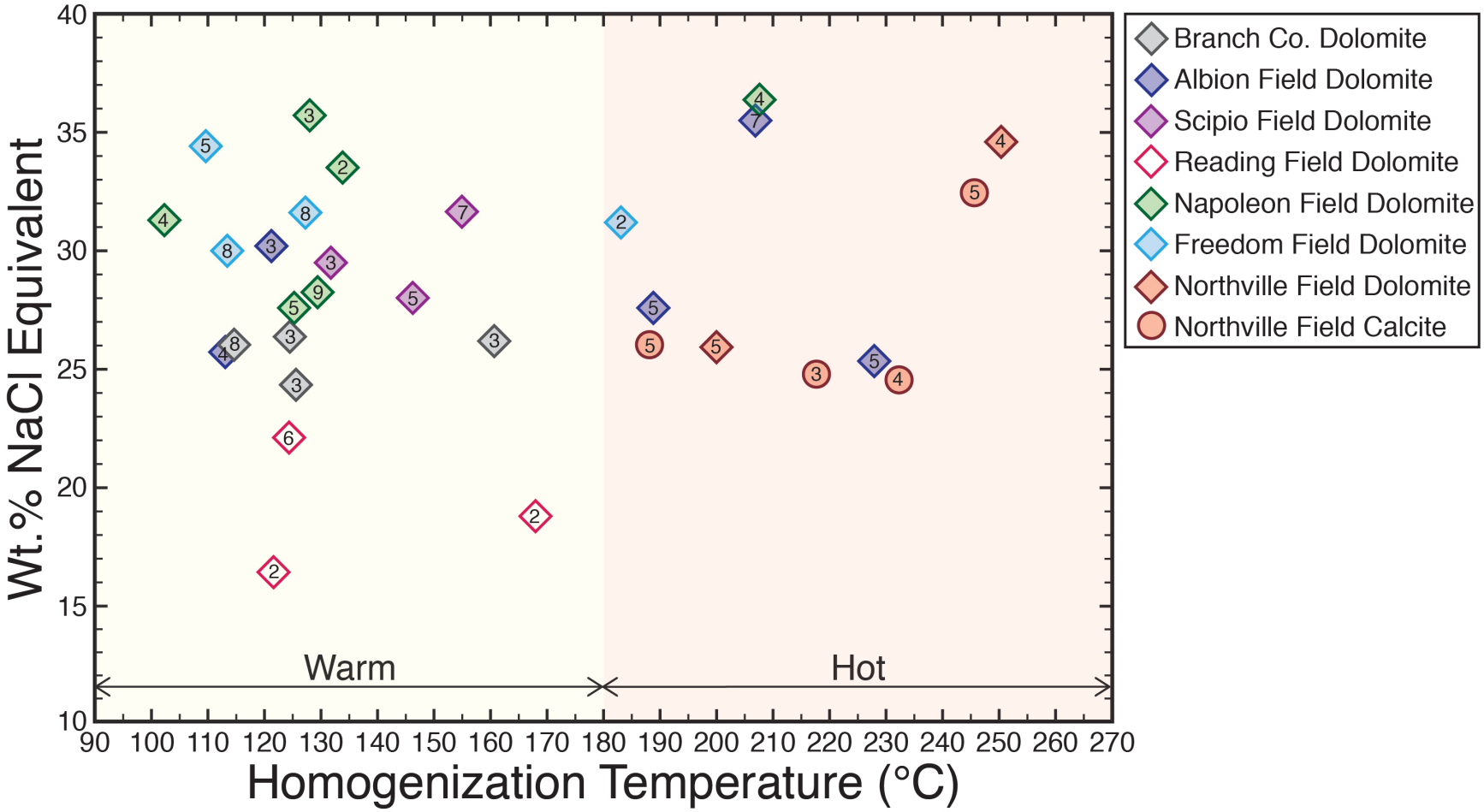

Figure 16: Fluid Inclusion Homogenization Temperatures (T_h) vs Salinity by assemblage. The number of individual fluid inclusions for which valid T_h and T_m values were measured are shown on each data point. These values were averaged to create one data point representative of the assemblage, which is plotted. Values are separated into two groups: warm (<180°C) and hot (>180°C).

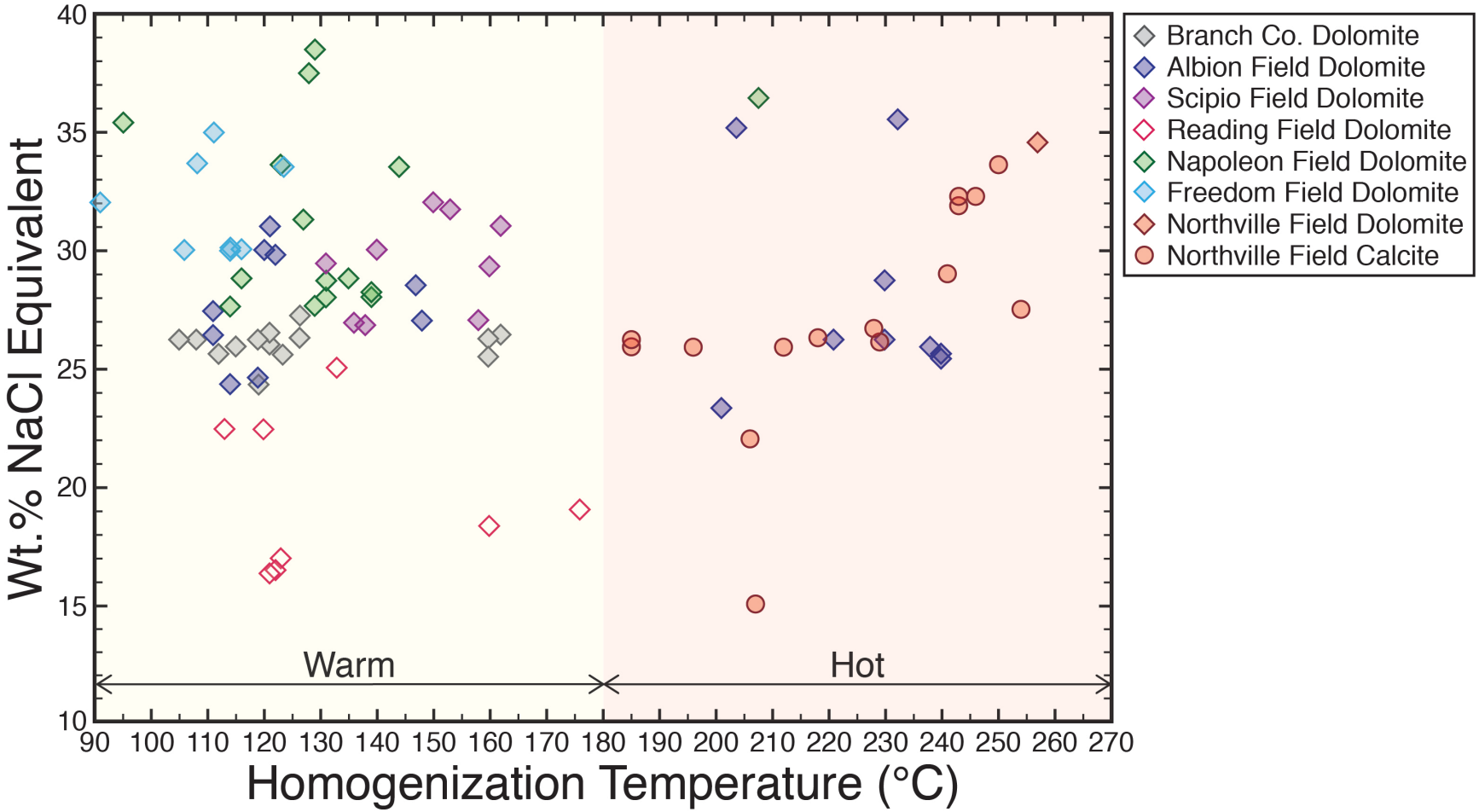

Figure 17: Fluid Inclusion Homogenization Temperatures (T_h) vs Salinity by individual data points. Only data points for which both a valid homogenization temperature (T_h) and last ice melt temperature (T_m) are plotted. Values are separated into two groups: warm (<180°C) and hot (>180°C) (same grouping as Figure 16).

Table 3: $\delta^{18}O$ and $\delta^{13}C$ Stable Isotope Data. Values of $\delta^{18}O$ and $\delta^{13}C$ plotted in figure 15. Location and sample lithology are noted.

Sample ID	Field	Depth	$\delta^{13}C$	$\delta^{18}O$	Lithology
121	Freedom	1150	-0.21	-8.38	Replacive Dolomite
122-1	Freedom	1214	-0.45	-7.86	Host Limestone
122-2	Freedom	1214	0.25	-8.10	Dolomite Cement
122-3	Freedom	1214	0.97	-8.07	Replacive Dolomite
123	Freedom	1224	0.41	-5.43	Host Limestone
124-1	Freedom	1230	0.85	-5.94	Host Limestone
124-2	Freedom	1230	0.87	-7.79	Replacive Dolomite
124-3	Freedom	1230	1.04	-6.22	Host Limestone
125	Freedom	1272	1.63	-5.84	Host Limestone
126	Freedom	1293	-0.59	-7.57	Calcite Cement
127-1	Freedom	1314	0.42	-7.07	Replacive Dolomite
127-2	Freedom	1314	0.41	-7.90	Dolomite Cement
128-1	Freedom	1341	0.82	-7.55	Replacive Dolomite
128-2	Freedom	1341	1.09	-7.57	Dolomite Cement
129-1	Northville	1261	-1.22	-8.88	Dolomite Cement
129-2	Northville	1261	0.00	-8.17	Replacive Dolomite
130	Northville	1286	0.06	-8.11	Replacive Dolomite
131-1	Northville	1348	0.28	-8.15	Replacive Dolomite
131-2	Northville	1348	0.22	-8.27	Dolomite Cement
132-1	Northville	1353	0.20	-8.55	Replacive Dolomite
132-2	Northville	1353	-0.94	-12.15	Calcite Cement
133-1	Northville	1360	0.40	-9.13	Replacive Dolomite
133-2	Northville	1360	-0.19	-9.66	Dolomite Cement
134-1	Northville	1365	0.84	-8.48	Replacive Dolomite
134-2	Northville	1365	-0.90	-10.57	Calcite Cement
135-1	Northville	1381	0.41	-8.32	Replacive Dolomite
135-2	Northville	1381	0.34	-8.28	Dolomite Cement
136-1	Northville	1390	0.93	-8.16	Replacive Dolomite
136-2	Northville	1390	-0.77	-12.34	Calcite Cement
137-1	Northville	1393	-0.23	-12.46	Calcite Cement
137-2	Northville	1393	0.61	-8.37	Dolomite Cement
137-3	Northville	1393	0.83	-8.20	Replacive Dolomite

Sample ID	Field	Depth	$\delta^{13}C$	$\delta^{18}O$	Lithology
138-1	Albion	1210	0.38	-8.46	Replacive Dolomite
138-2	Albion	1210	0.45	-8.50	Dolomite Cement
139	Albion	1216	0.36	-8.19	Replacive Dolomite
140-1	Albion	1252	0.14	-10.13	Calcite Cement
140-2	Albion	1252	0.24	-6.58	Host Limestone
141-1	Albion	1242	0.52	-7.08	Replacive Dolomite
141-2	Albion	1242	0.24	-7.41	Replacive Dolomite
142-1	Albion	1266	0.28	-7.41	Replacive Dolomite
143	Albion	1299	0.36	-7.65	Replacive Dolomite
144	Albion	1239	0.45	-8.15	Replacive Dolomite
145	Albion	1276	1.46	-6.45	Replacive Dolomite
146	Reading	955	0.31	-9.96	Replacive Dolomite
146-2	Reading	955	0.58	-9.98	Replacive Dolomite
147-1	Reading	965	0.39	-8.98	Replacive Dolomite
147-2	Reading	965	0.55	-6.59	Dolomite Cement
B 1	Scipio	1137	0.47	-8.79	Dolomite Cement
B10	Scipio	1175	0.24	-8.35	Dolomite Cement
B11	Scipio	1175	0.29	-7.63	Replacive Dolomite
B2	Scipio	1137	0.16	-8.14	Replacive Dolomite
B4	Scipio	1144	0.07	-8.58	Replacive Dolomite
B5	Scipio	1147	0.33	-8.33	Dolomite Cement
B6	Scipio	1150	0.47	-7.99	Dolomite Cement
B7	Scipio	1150	0.57	-7.67	Replacive Dolomite
B8	Scipio	1165	0.29	-8.58	Dolomite Cement
B9	Scipio	1165	0.36	-8.22	Dolomite Cement
M1	Scipio	1202	0.48	-8.84	Dolomite Cement
M2	Scipio	1202	0.85	-8.26	Replacive Dolomite
P1	Wildcat	997	0.01	-8.16	Dolomite Cement
P2	Wildcat	997	-0.21	-7.83	Replacive Dolomite
P3	Wildcat	1002	-0.11	-7.93	Dolomite Cement
P4	Wildcat	1002	-0.36	-6.76	Replacive Dolomite
P5	Wildcat	1000	0.10	-7.73	Calcite Cement
P6	Wildcat	1003	-0.33	-7.27	Dolomite Cement
W1	Napoleon	1240	0.67	-8.07	Dolomite Cement
W2	Napoleon	1240	0.57	-8.38	Replacive Dolomite

Sample ID	Field	Depth	$\delta^{13}C$	$\delta^{18}O$	Lithology
W3	Napoleon	1247	0.81	-8.11	Dolomite Cement
W4	Napoleon	1284	1.04	-8.85	Dolomite Cement
W5	Napoleon	1284	1.09	-8.21	Replacive Dolomite
W6	Napoleon	1285	0.86	-8.83	Dolomite Cement
W7	Napoleon	1290	1.02	-7.60	Dolomite Cement
W8	Napoleon	1290	0.88	-7.57	Replacive Dolomite
W9	Napoleon	1291	0.92	-6.94	Replacive Dolomite
W10	Napoleon	1291	1.02	-7.83	Dolomite Cement
W11	Napoleon	1294	0.87	-8.36	Dolomite Cement
W12	Napoleon	1294	0.87	-7.89	Replacive Dolomite
W13	Napoleon	1296	1.18	-7.78	Dolomite Cement
W14	Napoleon	1296	0.76	-6.79	Replacive Dolomite
W15	Napoleon	1302	0.56	-8.09	Dolomite Cement

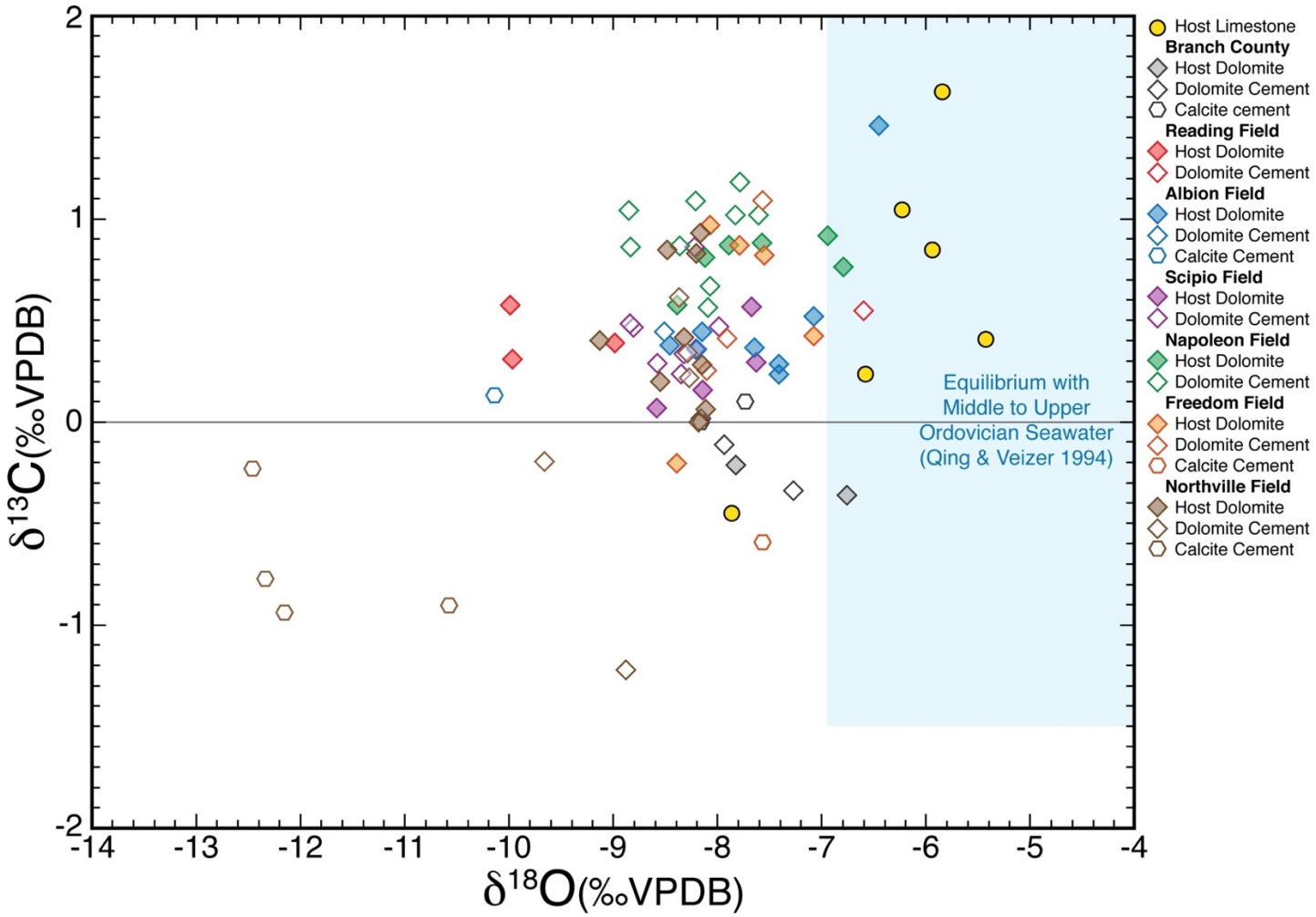

Figure 18A: $\delta^{18}O$ vs $\delta^{13}C$. Isotope values are color coded by locale. Color filled data points indicate host or replacive lithology, open shapes indicate void filling cements. Lithology is differentiated by shape. Data shows slight clustering by locale. All but 1 value for late cements are not in equilibrium with Middle to Upper Ordovician seawater (Qing and Veizer, 1994).

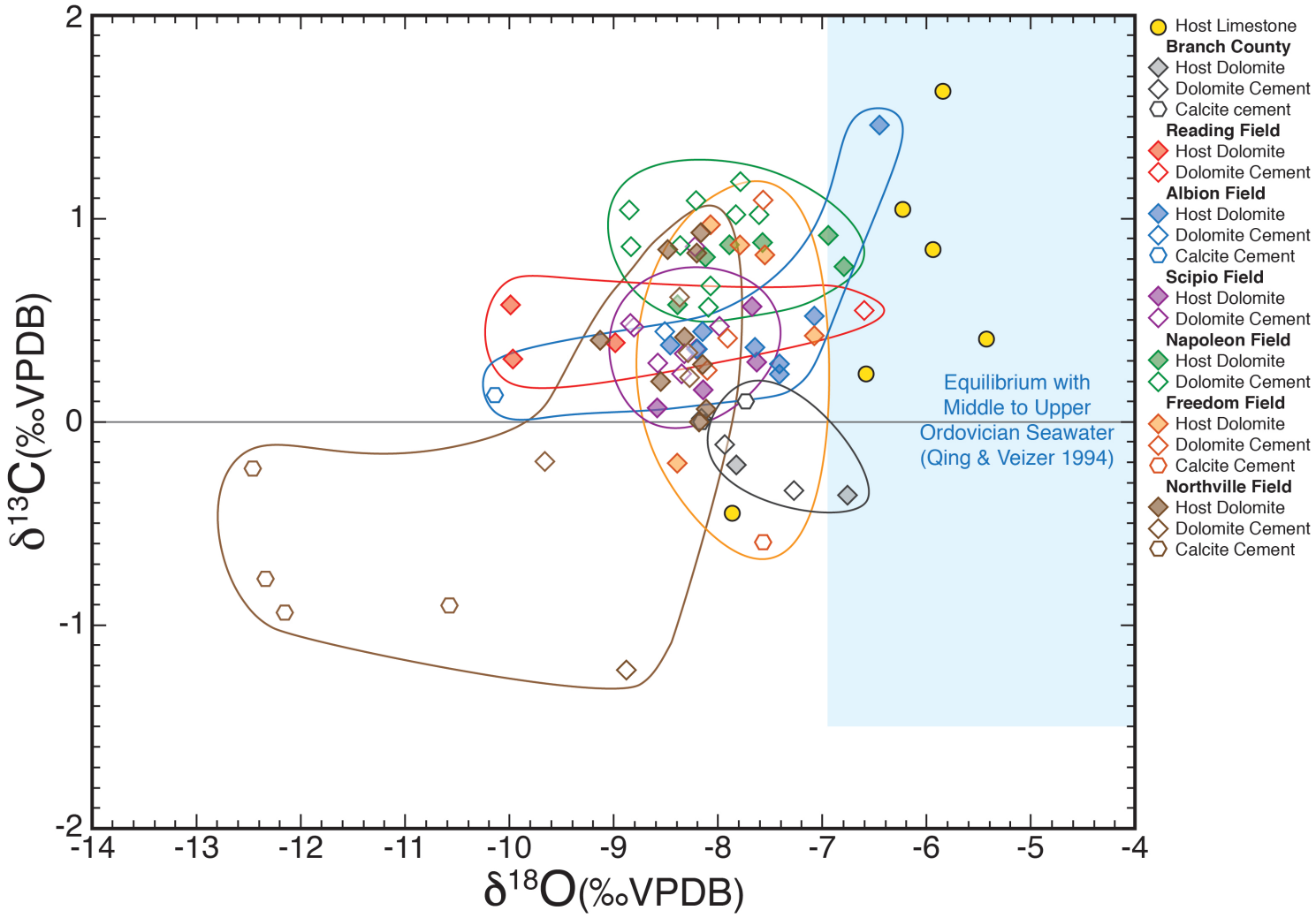

Figure 18B: $\delta^{18}O$ vs $\delta^{13}C$ with Field Cluster Outlines. Same data at Figure 18A with field clusters outlined to show overlapping data.

Table 4: $^{87}Sr/^{86}Sr$ and $\delta^{18}O$ Values by Field. Strontium values for samples in this study with corresponding lithology and oxygen isotope values.

Field	Sample #	$^{87}Sr/^{86}Sr$	Sr ppm	Cement Lithology	$\delta^{18}O$
Albion	86-144	0.7086	185.58	Dolomite (warm Th sample)	-8.15
Albion	86-138	0.7094	69.97	Dolomite (warmer Th sample)	-8.50
Branch County	P3291	0.7091	89.89	Dolomite	-7.27
Branch County	P3291	0.7091	133.06	Calcite	-
Freedom	86-127	0.7085	71.84	Dolomite	-7.90
Napoleon	WB4277	0.7085	3646.90	Dolomite	-8.17
Northville	86-132	0.7109	1128.65	Calcite	-8.55
Northville	86-132	0.7110	6223.93	Dolomite	-12.15
Reading	86-147	0.7088	813.95	Dolomite	-6.59
Scipio	M3940	0.7083	79.79	Dolomite	-8.84

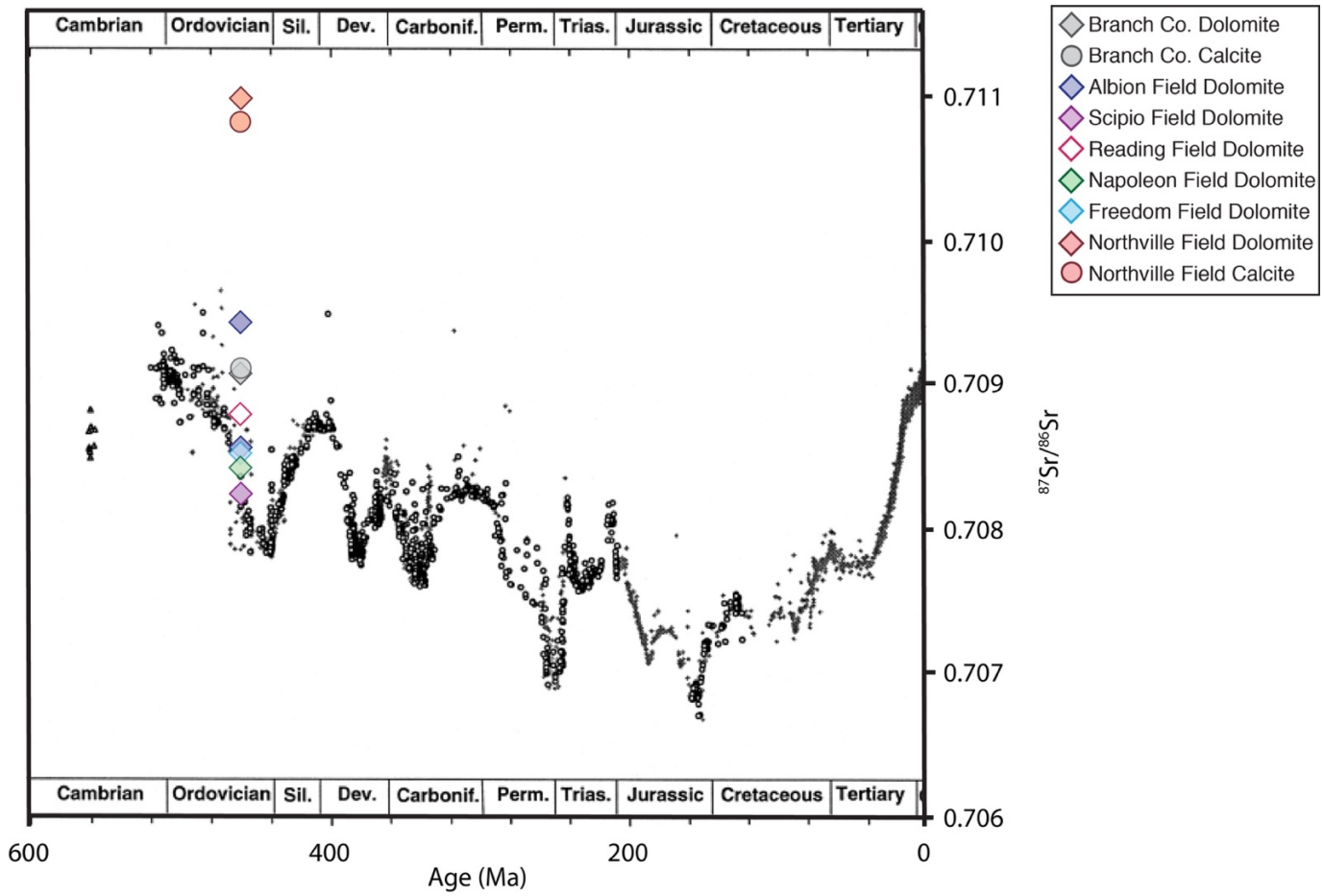

Figure 19: $^{87}Sr/^{86}Sr$ vs. Phanerozoic Seawater Curve. Values from this study overlap Middle Ordovician seawater and closely match Late Silurian seawater values. Northville oil field samples are an exception, indicating cement precipitating fluids interacted with basement sediments. One Albion sample (from a hot T_h sample) is high compared to Ordovician or Silurian seawater values, also suggesting interaction with basement sediments. After Veizer et al. (1999).

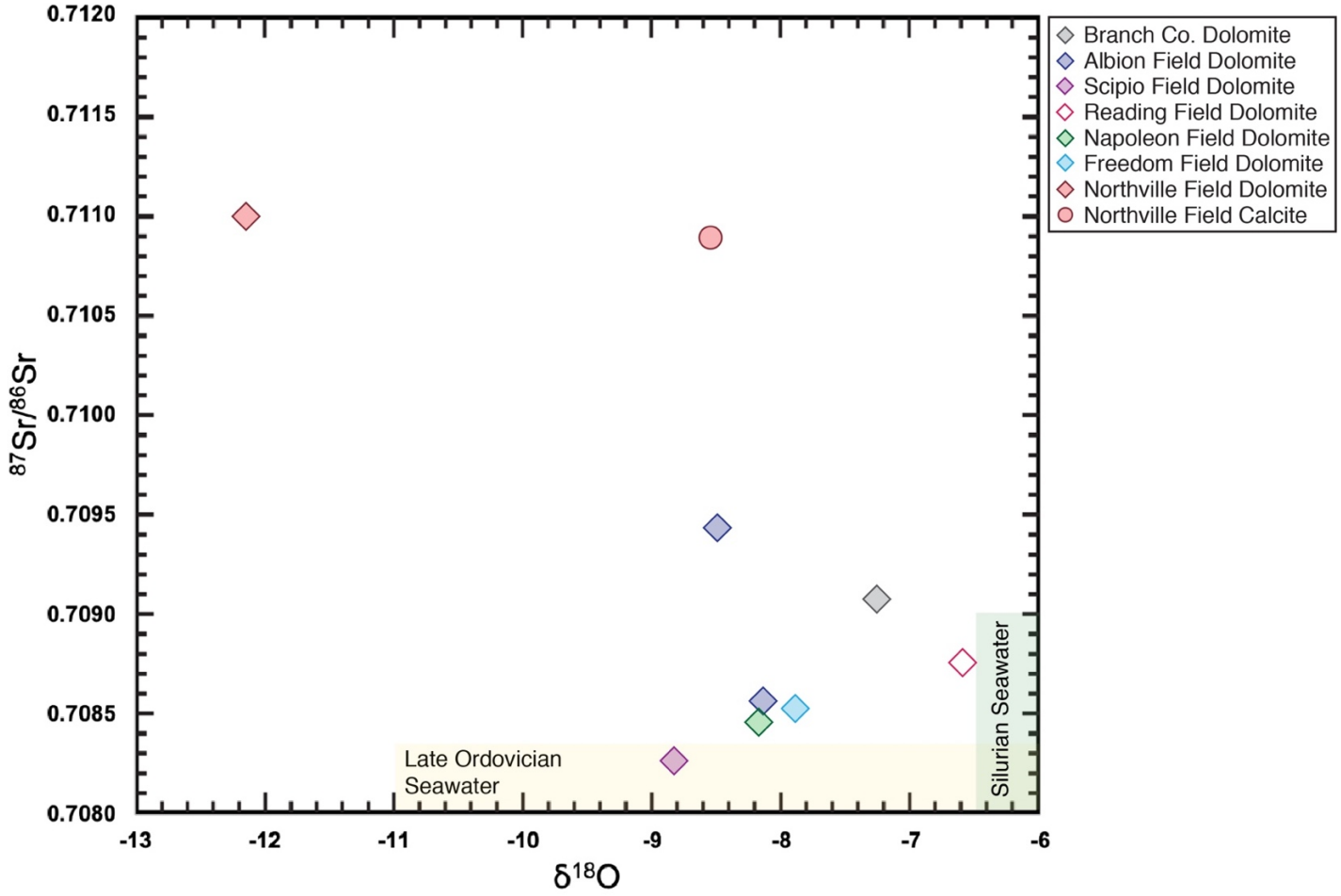

Figure 20: $^{87}Sr/^{86}Sr$ vs. $\delta^{18}O$. Expected values for Ordovician and Silurian rocks are plotted for comparison. Strontium values for Scipio oil field lie in the late Ordovician seawater field. Northville oil field strontium values lie above Ordovician and Silurian seawaters. Strontium values for all other oil fields studied lie in the range of Silurian seawaters. Values of $\delta^{18}O$ for all oil fields studied fall outside the range of expected normal Silurian seawater values. Estimated seawater range from Veizer et al. (1999) and Shields et al. (2003).)

CHAPTER V

INTERPRETATIONS

Petrologic Comparison Among Oil Fields

All of the oil fields studied here (Figure 4) display hydrothermal textures at the macro scale. Features observed in core include bedding plane and vertical fracture fill a few millimeters thick, vuggy porosity, collapse breccias, dolomite cement filling voids, zebra fabrics, and up to centimeter size saddle dolomite crystals in open space (Hurley and Budros, 1990; Wilson et al., 2001; Grammer and Harrison, 2013). Dolomite cements occur paragenetically after replacive dolomite. In the Northville field, void filling saddle dolomite cements are commonly followed by blocky calcite (Figure 8). In the Branch County core, dolomite cement is infrequently followed by blocky calcite, sphalerite, pyrite, and chalcopyrite . Wilson et al. (2001) recognized pyrite, barite, and calcite fracture fill in Northville oil field cores. They also observed fluorite and sphalerite in cores in the Albion-Scipio oil trend (Wilson et al., 2001). In the Trenton and Black River (TBR) of Ohio, Haefner et al. (1988) observed pyrite, sphalerite, marcasite, blocky calcite, gypsum and anhydrite. They suggest Michigan Basin brines as the source of cement precipitating waters in Ohio (Haefner et al., 1988). Calcite, anhydrite, pyrite, sphalerite, and fluorite paragenetically follow dolomite cements in the TBR of Indiana (Yoo et al., 2000). Bitumen coatings and hydrocarbon fluid inclusions in late cements are commonly observed in TBR oil fields (Haefner et al., 1988; Budai and Wilson, 1991; Coniglio et al., 1994; Yoo et al., 2000; Wilson et al., 2001). The mineral assemblages and paragenesis observed in this study and in literature (Figure 5) are

similar to late stage ore and gangue minerals observed in MVT deposits (Ells, 1962; Haefner, 1988; Hurley and Budros, 1990; Budai and Wilson, 1991; Allan and Wiggins, 1993; Wilson et al., 2001; Gregg and Shelton, 2012; Grammer and Harrison, 2013). This suggests cement precipitating fluids for dolomite reservoirs of the TBR are similar in composition to MVT ore fluids and may be the result of similar fluid flow systems.

Samples from all oil fields in this study, except the non-productive Branch County Core, have petroleum fluid inclusions in late void filling dolomite and calcite cements (Figure 15). These inclusions are commonly identified as primary and occasionally as secondary in healed fractures in matrix replacive dolomites and late dolomite and calcite cements. This indicates hydrocarbon migration occurred during hydrothermal fluid migration. Absence of petroleum inclusions in Branch County may be due to lack of organic-rich rock locally within the TBR sequence to provide a source, or insufficient time for warm fluids to generate hydrocarbons. Hydrocarbon generation followed by leak off in Branch County seems unlikely as no evidence of petroleum staining is observed in core or thin section (Figure 6A). The complex gangue assemblage observed in this core indicates cement precipitating fluids were not less mineralogically complex than others in the study.

If the oil fields studied here shared identical fluid histories, it should be possible to correlate CL 'stratigraphy' for late cements from field to field (Voss et al., 1980). This is not the case. Late diagenetic carbonate cements observed in each field display unique CL compositional zonation indicating unique fluid histories. The two fields with the most similar CL stratigraphy are the Albion and Napoleon oil fields (Figures 7B and 13B). The CL stratigraphy for late dolomite cement in both fields display a moderate CL inner core that gradually transitions to a

dull CL, and finally to non-CL response toward crystal edges. This change in CL response indicates a change in fluid composition during crystal growth. Iron is known to quench CL response (Machel, 1985), and different concentrations of iron are present in TBR late cements. This suggests that cement precipitating fluids became more iron rich as crystal growth progressed in the Albion and Napoleon oil fields and quenched CL response. The two oil fields are separated by approximately 50 km at the stratigraphic level of the TBR, but it is possible they share a connection of deep underlying basement structures or faults. A shared underlying structure would have allowed the same fluids to affect both fields simultaneously. Albion field dolomite cement is capped by an additional thin non-CL band (Figure 7B) which is absent in Napoleon (Figure 13B), so not all cement precipitating fluids were shared.

The Scipio oil field (Figure 10B), which appears to be a continuing trend with the Albion oil field to the north (Figure 4), also has a final dull to non-CL band. This suggests Scipio may have had partial sharing of fluid pathways and similar fluids and timing as the latest cement precipitating fluids affecting the Albion oil field. The Reading, Freedom, and Northville oil fields are geographically separate from the Albion-Scipio oil trend area by several tens of kilometers. These oil fields display unique cement stratigraphies suggesting that their underlying fault systems do not directly connect to other oil fields in the study. The Reading, Scipio, Freedom, and Northville oil fields display multiple CL bands in their void filling dolomite cements, possibly indicating that multiple fluids and/or fluid pulses were responsible for their precipitation. The Branch County core shows a single uniform, non-banded CL response in dolomite cements. This indicates either a single fluid is responsible for the dolomite cements, or the final fluid pulse dissolved any preexisting cements and reprecipitated a final cement phase. A single fluid event is

the more likely of these two hypotheses as no evidence of dissolution on crystal edges surrounding the final cements are recognized.

Despite lack of correlatable CL stratigraphy, similar processes are likely responsible for fluid movement and cement precipitation in all of the oil fields studied, and timing of fluid events are assumed to be similar. All oil fields studied display a similar gross mineral paragenesis (Figure 5), fluid inclusion microthermometry, and isotope geochemistry. Path-specific interactions are likely responsible for dissimilarities in CL stratigraphies.

Trends from Microthermometry

Salinities of included fluids in void filling carbonate cements in all of the oil fields studied are higher than those observed in other studies adjacent to the Michigan Basin (Haefner et al., 1998; Yoo et al., 2000; Smith, 2006; Patchen et al., 2006). The Branch County core and Reading oil field have the least saline included fluids, but still contain as much as 27.2 and 25.0% wt. NaCl, respectively (Table 2). Fluid salinity and complexity generally increase from west to east toward the Mid-Michigan Rift (MMR) (Table 2 and Figure 1). Eutectic values of included fluids measured in the Branch county core are among the highest in the study area at -63.8º C and eutectic values generally decrease to -112º C in Northville field which overlies a portion of the MMR. This trend of decreasing eutectic temperatures suggests an increase in divalent cation complexity toward the MMR. Homogenization temperatures also generally increase from west to east as the MMR is approached. The Branch County core homogenization temperature values are some of the lowest observed in this study at 79 to 130º C, while the Northville oil field carbonate cements display homogenization temperatures up to 258º C (Table 2; Figures 16 and 17). The

increased homogenization temperatures, increasing salinity trend, and decreased eutectic temperatures proximal to the MMR suggest it as a source of heat and higher salinity fluids. This warming trend may play a role in the variation observed in salinity if hot fluids were able to transport a higher volume of dissolved salt. Additionally, salt complexity may have been enhanced proximal the MMR as cations from basement rocks and basement derived sediments moved upward from the MMR during fluid transport events.

All of the oil fields studied contain a cluster of warm fluids with the exception of Northville, which displays hot values only, potentially due to its proximity to the MMR (Figures 16 and 17). This interpretation must remain tentative however, as values for both warm and hot fluid groups may exist in all fields in the study but were not observed. Albion is the only oil field in the study, which clearly displays evenly distributed warm and hot fluid clusters. Napoleon and Freedom oil fields each plot an assemblage data point on Figure 16 within the hot fluid field. The author interprets these as reliable data points, but they may be outliers for these oil fields. Average homogenization temperatures show a weak decreasing trend as oil fields become more distal from the MMR, again suggesting the rift as a source of heat.

Geochemical Evaluation

Stable carbon and oxygen isotope values for replacive dolomite and late void filling carbonate cements overlap previously published values for TBR in the Basin (Figure 18) (Taylor and Sibley, 1986; Haefner et al., 1988; Budai & Wilson, 1991; Coniglio et al., 1994; Yoo et al., 2000). Values for host limestone are largely consistent with calcite precipitated in equilibrium with Middle to Upper Ordovician seawater (Figure 18). All other carbonate $\delta^{13}C$ and $\delta^{18}O$ values

are more negative than calcite in equilibrium with Ordovician seawater. Calcite cement samples typically have more negative $\delta^{13}C$ and $\delta^{18}O$ values than dolomite cements from the same oil field. This is a typical response in hydrothermal fluids as elevated temperatures fractionate the heavier isotopes $\delta^{13}C$ and $\delta^{18}O$ in the fluid phase during precipitation (Land, 1980; Allan and Wiggins, 1993). Values of $\delta^{13}C$ and $\delta^{18}O$ also form clusters by field. Fluids likely had a common source, but interactions with surrounding rocks during transport along fault paths uniquely modified fluids in each field. If path-specific rock interaction did not play a part in fluid evolution, $\delta^{13}C$ and $\delta^{18}O$ values should overlap more evenly among fields with little evidence of field-specific clustering.

Carbonate cement precipitating basinal waters may equilibrate with host rocks or retain their source characteristics (Shelton et al., 2019). Values of $\delta^{18}O$ for cement precipitating waters were calculated utilizing $\delta^{18}O$ rock values and measured T_h ranges from fluid inclusions in this study to determine if equilibration with host rocks occurred prior to cement precipitation (Table 5). Dolomite values were calculated using Matthews and Katz (1977) and calcite values were calculated using O'Neil et al. (1969). Calculated $\delta^{18}O$ values for waters increase with higher temperatures (Land, 1980; Allan and Wiggins, 1993). This trend is commonly observed during calcite and dolomite fractionation due to temperature effects. If cement-precipitating waters were sourced locally or allowed to come into equilibrium with host rock prior to cement precipitation, calculated equilibrium values for cement precipitating waters and host limestone waters should overlap. They do not. Values of $\delta^{18}O$ for host limestone indicate isotopically light waters (-5.5‰ $\delta^{18}O_{VSMOW}$; Table 5) while calculated cement precipitating water values indicate isotopically heavy waters (+1.3‰ to +14.0‰ $\delta^{18}O_{VSMOW}$). Late Silurian seawater is isotopically similar to

Ordovician seawater with values near -5‰ $\delta^{18}O_{VSMOW}$ (Gódderis et al., 2001). This difference in $\delta^{18}O$ values highlights the highly evolved nature of cement precipitating fluids when compared to Ordovician and Silurian seawater. The broad range of calculated $\delta^{18}O$ values for cement precipitating waters (+1.3‰ to +14.0‰) in part reflects fractionation response across the broad range of homogenization temperatures (79 to 258º C) and supports conclusions from CL stratigraphy and fluid inclusion work that more than one fluid or evolving fluids precipitated the dolomite and calcite cements.

Values from $^{87}Sr/^{86}Sr$ analysis of void filling carbonate cements for oil fields in this study indicate influence by two fluids that were not Ordovician seawaters: Silurian seawaters, and basement waters (Figure 19). The range of $^{87}Sr/^{86}Sr$ values for Middle to Upper Ordovician (0.7078 to 0.7082) and Silurian (0.7078 to 0.709) seawaters largely overlap (Figures 19 and 20) (Qing et al., 1998; Veizer et al., 1999; Shields et al., 2003). Strontium isotope values for the Reading, Freedom, Scipio, Napoleon, and the Albion oil field samples containing warm fluid inclusion values (0.7083 to 0.7088) are slightly more radiogenic than Upper Ordovician values (Figure 19). This could be explained by fluids buffering with local Lower to Middle Ordovician carbonates (0.7088 to 0.7092) (Shields et al., 2003). However, high salinities of included fluids strongly suggest Silurian Salina Group evaporite influence on fluids in cement precipitating waters. Values of $^{87}Sr/^{86}Sr$ in these oil fields overlap published values (Veizer et al., 1999; Shields et al., 2003) for late Silurian seawaters (0.7083 to 0.709), suggesting that fluids with dissolved Salina Group evaporite compositions are a major component of the cement precipitating waters. Cement precipitating fluids sourced from Silurian evaporated seawaters are the most likely

explanation for both the high salinity of included fluids and strontium values measured in carbonate cements in these oil fields.

Measured values of $^{87}Sr/^{86}Sr$ for carbonate cements higher than expected Ordovician or Silurian seawater values suggest involvement with granitic basement or basement derived sediments. The hot Albion cement value, and both Branch County cement values have $^{87}Sr/^{86}Sr$ value that are higher than Silurian seawater values (0.7094 and 0.7091, respectively) (Figure 19). These higher $^{87}Sr/^{86}Sr$ values are consistent with fluids that have circulated through basement or basement derived sediments to attain $^{87}Sr/^{86}Sr$ ratios above those of Silurian and Ordovician waters (>0.7090). These fields may have a more direct connection to basement through their underlying fault-fracture network than other fields that were studied allowing deeply sourced basement brines to move into the TBR. The Branch County core is unusual in that it contains radiogenic strontium indicating fluids likely moved through basement, but relatively low fluid inclusion homogenization temperatures relative to other oil fields in this study.

Highly radiogenic values of $^{87}Sr/^{86}Sr$ in the Northville oil field cements (0.7109 to 0.7110) are likely due to the strong influence of continental basement on deeply circulating fluids (Figure 19). Northville oil field cements also have the highest homogenization temperatures measured in this study (Table 2; Figures 16 and 17). Basement influence for all fields in this study cannot be ruled out. Strontium values measured in this study may be a combination of Silurian seawater, basement influence, and buffering with Ordovician carbonates. Because of these complex interactions, strontium values that fall within Silurian and Ordovician values (0.7078 to 0.709) (Qing et al., 1998; Veizer et al., 1999; Shields et al., 2003) do not necessarily preclude fluids traveling through basement sediments.

Strontium isotope results across the study area are mixed regarding basement involvement (Figure 19). Similarly, mixed results exist for $^{87}Sr/^{86}Sr$ in the literature. Values from Haeri-Ardakani et al. (2013) (0.7087 to 0.7091) are interpreted by the authors to indicate basement involvement. Values from Granath (1991) (0.70834 to 0.70898) and Allan and Wiggins (1993) (~0.7084 to 0.7091) are interpreted by the authors to suggest Silurian influence only. Values from McNutt (1987) (0.70901 to 0.71041) and Hobbs et al. (2011) (0.70929 to 0.71045) are not specifically interpreted by the authors as favoring or opposing basement influence, but values above 0.709 are interpreted in this study as basement influenced. Values for $^{87}Sr/^{86}Sr$ above those expected for Ordovician values indicate some degree of water-rock interaction has taken place. Combined with T_h values that require heat above that expected for Ordovician and shallower rocks based on thermal gradients alone, movement through basement sediments is a reasonable assumption for included fluids observed in fault-fracture oil fields in south-central Michigan.

Origin and Evolution of Fluids

Source of Salt

Fluid inclusion data indicate complex and highly saline fluids affecting all of the oil fields studied. Eutectic values (T_e) for included fluids are far below that of a simple H_2O–NaCl system indicating the presence of $CaCl_2$ and other salts. This is consistent with the findings of previous studies (Granath, 1991; Allan and Wiggins, 1993; Hobbs et al., 2011; Nurkhanuly, 2012). Ratios of Cl/Br measured by Hobbs et al. (2011) in the TBR of Ontario provide strong evidence that dolomitizing waters were sourced from seawater evaporated beyond halite

saturation. The most likely source of halite saturated brines in the Michigan Basin is the overlying Silurian Salina Group evaporite units. The Salina Group contains thick sections of evaporites including gypsum and halite as well as sylvite (KCl) near the center of the Basin (Catacosinos et al., 1990). Analysis of current TBR produced waters indicates that Silurian salts are a major component of these waters (Allan and Wiggins, 1993). The lowest T_e values (-112º C) measured in this study come from the Northville field indicating that more highly complex fluids were present during cement precipitation here than in the other oil fields studied. Cations from crystalline basement rocks were likely transported along faults contributing to Na-Ca-Mg-Cl brines in the Northville oil field area (Allan and Wiggins, 1993; Hobbs et al., 2011). Northville's proximity to the MMR suggests the rifted basement as the source for these cations.

Source of Heat

Uncorrected T_h values trend higher from the coolest in the Branch County core (79 to 130 º C) eastward to the warmest Northville field values for calcite and dolomite cements (163 to 258º C) (Figures 1, 16, and 17). This trend suggests a source of heat proximal to Northville field. The Northville oil field lies immediately above the MMR and higher heat values near the thinned crust over the rift is a likely source for the hot fluids observed there (Figure 1). Diminishing heat values distal from the rift would form similar decreasing T_h values as observed in this study (Figures 1, 16 and 17).

Fault-fracture hydrothermal systems are affected by upward moving warm fluids (Allan and Wiggins, 1993; Machel and Lonnee, 2002; Gregg and Shelton, 2012). The present-day geothermal gradient for the Michigan Basin is 19.2º C/km and current temperatures of TBR rocks

are 40º C at an average depth of 1250 m (Vugrinovich, 1988). Oils in the TBR are likely generated *in-situ* from organic rich carbonates and shale layers within the interval, which can be up to 20 to 25% total organic carbon, or from the immediately overlying Utica shale (Reed et al., 1986). *In-situ* oil generation could not have occurred at current geothermal gradients and depths. To explain the presence of oil and other thermal maturity indicators in the Michigan Basin, geothermal gradients of up to 56º C/km are cited if no additional overburden is assumed (Moyer, 1982; Vugrinovich, 1988). Thermal gradients in strike-slip basins can be as high as 200º C/km—much higher than those expected in intracratonic sag basins (Allen and Allen, 2013). The Michigan Basin overlies a failed rift, and may have had higher temperature gradients during the early Paleozoic Era. These temperature gradients would be more similar to those of faulted or strike-slip basins. Heat associated with the underlying MMR could increase past temperature gradients enough to account for elevated temperatures within the Basin without the need for additional overburden or burial. However, Lopatin models run by Cercone (1984), using data from Moyer (1982), estimate an additional 1000 m of sediment existed in the Basin between the Permian and Jurassic that has since been removed. This additional 1000 m combined with the 700 m remnant of Jurassic Red Beds in the Basin center closely match the 1800 m of sediment observed over this same interval in the adjacent Illinois Basin (Cercone, 1984). In the extreme case, maximum burial temperatures for Ordovician rocks near Basin center could be as high as 232º C using 4 km maximum burial from Cercone (1984), the maximum suggested geothermal gradient of 53º C/km from Moyer (1982), and an ambient surface temperature of 20º C. Most authors (Cercone, 1984; Nunn et al., 1984; Vugrinovich, 1988; Cox, 2015) favor a more moderate 35 to 45º C/km gradient, placing maximum burial temperature in Middle Ordovician rocks from 160 to 200º C near Basin center. Even in the extreme case at Basin center, homogenization

temperatures in the hot oil fields studied here are tens of degrees warmer than temperature estimates for burial alone. Additionally, oil fields of south-central Michigan were less deeply buried than the basin center and would have attained lower maximum burial temperatures. During the late Silurian, oil fields of south-central Michigan resided at ~0.5 km depth (Cercone, 1984). Using this depth, and the surface temperature and gradients from above (20º C and 35 to 45º C/km), ambient burial temperatures would have been 37.5 to 42.5º C. Homogenization temperatures, assuming cement precipitation during late Silurian, are at least 36.5º C warmer (Branch County minimum 79º C) and up to 220.5º C warmer (Northville maximum 258º C) than ambient burial temperatures (Table 2, Figures 16 and 17). Pressure corrections for cement precipitation during late Silurian increase filling temperatures for fluid inclusions an additional 5º C above measured homogenization temperatures (Table 6). If cement precipitation occurred at maximum burial (~2km depth for the south-central Basin, from Cercone, 1984), ambient temperatures would be 90 to 110º C and only the lowest uncorrected values from Branch County and the Reading, Albion, Napoleon, and Freedom oil fields could be explained by burial temperatures. Pressure corrections at this depth increase filling temperatures on average by 22º C (Table 7). Corrected values raise all measured homogenization temperatures for cements above ambient background temperatures at maximum burial. Even without pressure corrections, additional heat is needed above the expected 35 to 45º C/km temperature gradients to obtain the hot T_h values in all oil fields studied.

There are two likely sources for the excess heat in the southern Michigan Basin: a heating event in the Basin raising temperatures *in-situ*, and/or sourcing fluids from deeper, hotter rocks. Additional thermal anomalies throughout the Michigan Basin's history have been suggested

(Nunn et al., 1984; Catacosinos et al., 1990; Howell and van der Pluijm, 1999), but are not definitive, and even the highest suggested geothermal gradient (Vugrinovich, 1988) cannot produce the homogenization temperatures observed in all the oil fields studied. However, hot fluids moving upward along faults from deeper in a basin are a commonly recognized mechanism for cement precipitation in hydrothermal regimes (Machel and Lonnee, 2002). Assuming the moderate temperature gradients from above (35 to 45º C/km), fluids of 260º C could be sourced from depths of 5.3 to 6.9 km. The base of the TBR is ~0.5 km from basement. To obtain heat values recorded in this study with no mechanism other than burial temperatures, fluids must have circulated 500 m or more into basement rocks even at maximum burial.

Fluid Movement

Thermal convection, topography driven flow, and seismic pumping, or a combination thereof, could be at play in the Michigan Basin (Muir-Wood and King, 1993; Garven, 1995; Hobbs et al., 2011). Based on evidence from this study, a fault-controlled convective model is suggested for dolomitizing hydrothermal fluids in the south-central Michigan TBR oil fields. This is similar to the deep-convection fluid flow model for MVT deposits described by Gregg and Shelton (2012) in which cool, dense fluids descend down fault paths to basement where they are heated, leach metals and salts, then reverse direction and ascend up faults, losing heat and precipitating cements (Person and Garven, 1992; Garven and Raffensperger, 1997). This study and others (Allan and Wiggins, 1993; Hobbs et al., 2011) suggest waters sourced from the Silurian Salina Group are a major component of dolomitizing fluids for TBR reservoirs. Therefore, fluid movement downward can have occurred no earlier than Middle to Late Silurian and puts a lower boundary on the age of TBR cements. Initial fluid movement downward from

Salina Group evaporites was likely density driven and facilitated by existing fault-fracture networks (Allan and Wiggins, 1993). This implies fault fracture networks were already in place at Silurian time (TBR burial depth ~500 m), or formed at this time. The Iapetus Ocean was continuing to close during Silurian time as Baltica and Laurentia were converging to form Laurussia in the Caledonian orogeny (Ettensohn, 2004). There is evidence in the nearby Appalachian Basin from structural reactivation and Silurian-Devonian magmatism to suggest Salinic (Silurian) tectonism continued intermittently into the neo-Acadian orogeny (Ettensohn, 2004). These events may have formed fault and fracture pathways during and shortly after Salina Group deposition. Inter-seismic dilation may have assisted in drawing fluids down to basement level especially near extensional bends in underlying wrench faults (Muir-Wood and King, 1993). Versical (1991) studied shear and structural feature orientations in the Albion-Scipio trend and Stoney Point fields. Left-lateral strike-slip on underlying basement faults created fractures (Riedel shears) in the overlying section, which produced extensional features (Versical, 1991). These extensions and bends along the strike-slip faults in the basement, would act as low pressure areas and essentially pull fluids downward to fill them (McCaig et al., 2000). Once highly saline fluids had traveled deeply into the basement to be heated, they likely reversed direction and moved upward through the rock column driven by convection and/or seismic pumping. Collapse of extensions in underlying basement faults during reactivation and closure in response to strike and oblique slip would rapidly expel fluids upward from the basement (Muir-Wood and King, 1993). These expulsions would occur at similar, but slightly different, times and locations (Wendte et al. 2009). These slight differences would help explain variances in geochemical signatures by oil field seen in the data. Wrench faulting in strata as young as the Devonian and Mississippian is recognized in the Basin (Ells, 1962). These fault networks provide a path for fluid flow upward

from deeper, higher temperature rocks into shallower, cooler rocks and suggest multiple episodes of fault reactivation throughout the Basin's history. Fluids in sedimentary basins are known to transfer heat and mass over large distances in short timeframes (Bethke, 1986; Garven 1995). Because of this, high geothermal gradients may not be required in the Basin if cement precipitating fluids transported heat from the basement during their upward movement and this heat was recorded by entrapped fluids in cements. Temperatures estimated from conodont color alteration are higher in samples in Albion-Scipio hydrocarbon producing zones than for those from surrounding unaltered limestones (Catacosinos et al., 1990). Fractures heat their surroundings through advection instantaneously, but conductive heat flow away from a fracture is extremely limited (Allan and Allan, 2013). This supports the idea that fluids transported heat along existing fault-fracture pathways into TBR oil fields and explains higher temperature values close to faults and rapid decreases in temperature away from fault-fracture systems.

Independent fault-controlled convective systems explain observed T_h values, slight variations in stable isotope values, differences between observed $^{87}Sr/^{86}Sr$ values in cement and expected Ordovician $^{87}Sr/^{86}Sr$ values, and differences in CL stratigraphy for each oil field. Oil fields with separate fault-fracture systems, even when sourced from the same fluid reservoir, would display slightly different homogenization temperatures, eutectic temperatures, salinities, and $^{87}Sr/^{86}Sr$ values due to unique path interactions through the rock column. Differences in homogenization temperatures and $^{87}Sr/^{86}Sr$ values are explained by the depth to which fluids traveled into the basement. Fluids that traveled more deeply into the basement would have a longer path to obtain radiogenic strontium, and have been heated to higher temperatures than fluids that stopped at more shallow depths. Residence time in the basement could also be a factor

affecting strontium values and concentrations. Fluids that traveled rapidly from heated depths to cement precipitation sites would also record warmer homogenization temperatures than fluids that traveled more slowly, losing heat in transit prior to cement precipitation in the TBR. Path specific interactions explain slight differences in $\delta^{13}C$ and $\delta^{18}O$ values and CL patterns. Independent fault systems for each oil field would reactivate at slightly different times and with varying intensities. This variance would change the number, and potentially thickness, of compositional zones (CL bands) in carbonate cements. Oil fields that share partial paths or connected fault systems would show similar fluid histories, but vary from each other slightly due to variations in fluid pathways.

Invasion of heated fluids from underlying rocks also explain the presence of petroleum in late cements in TBR oil fields. If cement precipitation occurred during or near Silurian time, burial temperatures calculated above (37.5 to 42.5º C) are not high enough produce oil. Values for T_h in all oil fields studied are above the lower limit for oil generation (60º C) so basement heated fluids that generated cements could also force maturation and generate and transport oil. A similar model for petroleum generation is cited by Jaiswal et al. (2019) as potentially responsible for oil in Mississippian limestone in a structural depression in Payne County, Oklahoma. If cement precipitation occurred later, when Ordovician rocks were sufficiently buried to generate oil in-situ, cement precipitating fluids could transport hydrocarbons and entrap them in included fluids. The Branch County core displayed some of the lowest temperatures measured for included fluids, but values are still above the lower limit for oil generation. Insufficient time for maturation by hot fluids or lack of organic-rich source material in this area may have precluded oil generation.

A fault-controlled convective model for fluid evolution is favored over a fluid mixing model for fluid histories. In a mixing trend, end member fluids blend and form a linear trend of fluid properties between them. If a mixing trend were responsible for fluid evolution in south-central Michigan, one would expect a warmer, less saline fluid from below mixing with a cooler, more saline fluid from above. A semi-linear trend in fluid inclusion values between these two end members should be recognizable. Calcite and dolomite cement fluid inclusions in the Irish Midlands (Wilkinson et al., 2005; Johnson et al,. 2009; Wilkinson et al., 2010; Shelton et al., 2019) and quartz cement hosted inclusions in the Reef Deposit in the Wisconsin Wausau Volcanic Complex (Haroldson et al., 2018) provide examples of fluid mixing trend patterns in microthermometry data. This pattern is not observed in cements of the south-central Michigan Basin. Rather, fluid inclusions in this study display distinct clusters of warm (~110 to 175º C) and hot (~180 to 250º C) T_h values (Figure 16 and 17). These two clusters have similar salinities, suggesting dolomitizing fluids had similar salinities, and slightly different histories for heating.

The overlapping clusters of isotope values in this study also argue against a mixing trend (Figure 18). Fluids sourced from distinct end member fluids, especially those with large temperature variations, cluster as separate groups when plotted. The higher temperature fluid tends toward more negative values for $\delta^{13}C$ and $\delta^{18}O$, with an especially strong tendency toward light $\delta^{18}O$ due to temperature-controlled fractionation effects. The cooler fluid shows an opposite, less negative trend. Mixing of these end member fluids typically would form a trend of data points from one end member to the other. Fault-fracture dolomitization of Mississippian rocks along the North Dublin (Ireland) coast provide a good example of the effect of mixing fluids on stable isotope data (Shelton et al., 2019) that is not observed in the TBR of the Michigan Basin.

Basin-wide and Regional Comparison

Salinity calculations in the literature (Granath, 1991; Allan and Wiggins, 1993) for the Albion, Scipio, Stoney Point, Reading, and Northville oil fields closely agree with those calculated for this study. All values were highly saline, 32.8 – 38.1 wt. % NaCl equivalent, and complex, with authors advocating an evaporated Silurian seawater component (Granath, 1991; Allan and Wiggins, 1993). Fluid inclusion measurements made outside of, but adjacent to, south-central Michigan are generally less saline. Included fluids in TBR carbonate cements in Ontario and Ohio are near 20 wt. % NaCl (Haefner, 1986; Patchen et al., 2006). Fluids in eastern Wisconsin for sphalerite, dolomite and quartz cements range from 14 to 26 wt. % NaCl (Luczaj, 2001). All eutectic temperatures inferred from first ice melt by Luczaj (2001) were near -57º C and brine compositions from crushing analysis (Na-Ca-Mg-Cl) were similar to those observed in Ordovician rocks of the Michigan Basin. Included fluid salinities in Indiana TBR dolomite cement samples nearest the study area are as high as 30.2 wt. % NaCl with T_e averaging -52.1º C (Yoo et al., 2000). All of these measurements (Ontario, Ohio, Wisconsin, and Indiana) indicate that highly evaporated, complex salts are a volumetrically important component of dolomitizing brines with most authors citing Silurian Salina Group evaporites as the source of salt (Granath, 1991; Allan and Wiggins, 1993; Luczaj, 2001). Salinity values distal from the Michigan Basin are lower than those on the Basin margins with salinities in New York averaging 15 wt. % NaCl (Smith, 2006). Salinities for included fluids in Cave-in-Rock MVT minerals in southern Illinois are 22 wt. % NaCl in fluorites and drop to 9.3 wt. % NaCl in quartz cements (Hall and Friedman, 1963). In the Upper Mississippi Valley district of Wisconsin and northern Illinois, calcite inclusions are only 5.5 wt. % NaCl (Hall and Friedman, 1963). Hall and Friedman (1963)

estimated ore emplacement temperatures at 75 to 130º C, with an initially connate water for Cave-in-Rock fluids followed by a later magma heated fluid pulse. They also suggest connate water flushing is responsible for Upper Mississippi Valley calcites (Hall and Friedman, 1963). Salinities and predicted ore emplacement temperatures for Cave-in-Rock and Upper Mississippi Valley fluids are lower than those observed in the south-central Michigan Basin (Hall and Friedman, 1963; Haefner, 1986; Granath, 1991; Allan and Wiggins, 1993; Luczaj, 2001; Yoo et al., 2000; Patchen et al., 2006; Smith, 2006; Hobbs et al., 2011; Nurkhanuly, 2013; this study). These lower salinities and temperatures indicate processes involved in brine enrichment affect the central Michigan Basin area more strongly than those distal from the Basin. Potentially, hot fluids (up to 250º C) in the central Basin area were able to hold in solution and transport larger volumes of salt. Basement-connected faults in south-central Michigan may have played a crucial role in salt and heat transport. Additionally, thick sections of overlying Silurian Salina Group evaporites add to salt concentrations and complexities in Michigan Basin fluids.

In Wisconsin and northwestern Michigan Devonian Dundee Formation hydrothermal reservoirs have many characteristics similar to TBR reservoirs including hydrothermal dolomite fabrics, MVT mineral assemblages, and association with basement connected faults (Luczaj, 2006). Void filling dolomite cements also commonly display inclusion-rich cores and limpid, inclusion-poor rims similar to those in TBR reservoirs (Luczaj, 2001). Fluid inclusions in Dundee dolomite cements have nearly identical salinity ranges (34 wt. % NaCl average) and T_e (-64º C) values as in the TBR of this study (Luczaj et al., 2006). Luczaj et al. (2006) conclude Silurian Salina Group salts are responsible for the heavy, complex brines associated with void filling dolomite cements in the Dundee Formation. In this case, warm saline brines from the

stratigraphically lower Salina Group traveled up brittle fault surfaces during hydrothermal events in nearly identical fashion to those proposed here for brines that formed TBR cements. The striking similarity between the Dundee and TBR fluids in salt concentration and eutectic temperatures suggests a common source of salt for both cements.

Values of T_h measured for this study exceed those of previous studies for the south-central Michigan Basin, on the Basin edges, and nearby equivalent strata in the Appalachian Basin (Haefner, 1986; Granath, 1991; Allan and Wiggins, 1993; Luczaj, 2001; Yoo et al., 2000; Patchen et al., 2006; Smith, 2006; Hobbs et al., 2011; Nurkhanuly, 2013). These hot (>180º C) fluids appear to only be affecting fields in the south-central part of the Basin, but data for central and north-central Michigan are lacking and the observed warming trend may continue northward from fields in this study. Maximum T_h values for TBR rocks in New York, Ontario, Indiana, Wisconsin and Ohio range from 108 to 180º C (Haefner, 1986; Granath, 1991; Allan and Wiggins, 1993; Luczaj, 2001; Yoo et al., 2000; Smith, 2006; Hobbs et al., 2011; Nurkhanuly, 2013). In Ontario, Coniglio et al. (1994) observed maximum T_h values of 220º C; the highest observed value in literature for the Michigan Basin prior to this study. However, values from the Albion and Northville fields in this study were tens of degrees warmer still (up to 258º C; Figures 16 and 17). Different processes must be affecting the oil fields in the south-central part of the Michigan Basin compared to the surrounding region.

Values of T_h measured in this study generally increase toward the MMR with the exception of the hot fluid inclusion group in the Albion field (Figure 1 and Table 2). Clusters of hot fluid inclusion values in a field distal from, but still relatively near, the MMR could be explained by a direct connection to basement sources through which fluids moved rapidly upward

with minimal heat loss. Additionally, increasing T_h values from west to east likely indicate warmer temperatures in the east of the Basin, or a source of heat east of the Basin boundary. Citing a source of heat east of the Basin should produce temperatures in Ontario near or above those observed in the Northville field, the eastern-most oil field in this study. As discussed above, maximum homogenization values in Ontario (220º C) are still far lower than observed values in Northville oil field (258º C), so this situation seems unlikely.

The Taconic, Acadian, and Alleghanian orogenies may have influenced fluid evolution in the Michigan Basin and timing of these events is favorable to suggested timings for hydrothermal fluid events in the Michigan Basin (Hobbs et al., 2011; Nurkhanuly, 2012; Haeri-Ardakani et al., 2013). Large regional tectonic events would explain increased geothermal gradients and reactivation of basement faulting. Reactivation of basement faults could also provide a mechanism for moving warmed fluids quickly from basement level to Ordovician strata. Caledonian, Acadian, and Alleghenian events are coincident with or post-date Silurian Salina Group deposition, the lower constraint on timing of dolomitization suggested by this study and others to explain observed salinity values and complexity (Hurley and Budros 1990; Granath, 1991; Allan and Wiggins, 1993). K-Ar ages of illites in the St. Peter and Glenwood sandstones in the Basin have been reset, with youngest ages nearest and overlying the MMR (Girard and Barnes, 1995). Values were likely reset by a renewed heating event in the rift elevating geothermal gradients to 34º C/km or higher and these ages indicate a Late Devonian to Mississippian event (Girard and Barnes, 1995). This event has similar timing to Acadian reactivation. Emplacement of Pb-Zn MVT deposits in the Silurian of southern Ontario are believed to be late Paleozoic to early Mesozoic and coincident with dolomitization of TBR

reservoirs (See Hobbs et al., 2011 and references therein). This event suggests the Alleghenian orogeny may have influenced reactivation of the MMR and faults underlying TBR oil fields and thus, dolomitization of TBR reservoirs. It is also possible the regional orogenies played no role in fluid evolution and movement in the Michigan Basin. Rather, a renewed basement heating event could increase thermal gradients locally and heat basement fluids to induce a hydrothermal system. No direct evidence of a renewed mantle heating event is currently recognized (Sleep et al., 1980) so further study would be needed to advocate a mantle heating event as the sole driver for fluid heating and movement responsible for cement emplacement in TBR Ordovician reservoirs. However, work by Luczaj (2001) suggests a regional pattern of outward flow from the Michigan Basin into surrounding margins in all directions during the middle Paleozoic, which favors upwelling and expulsion related to heating. Events in the basin do not directly correlate with any single orogeny suggested here, and it seems likely that fault dilation and closure in the basin remained active episodically throughout the Paleozoic facilitating fluid movement and cement precipitation.

CHAPTER VI

CONCLUSIONS

Fluid histories for fault-fracture oil fields in the Middle Ordovician Trenton and Black River (TBR) formations of the southern Michigan Basin are complex. From the data presented in this study, the following conclusions have been drawn.

Homogenization temperatures indicate a warm fluid less than 180º C and a hot fluid greater than 180º C were present during cement precipitation. The hot fluids (>180º C) appear to only be affecting oil fields of the south-central Michigan Basin, but data for central and north-central portions of the Basin is lacking, so the hot fluid trend may continue. Trends from homogenization data point to the Mid-Michigan Rift (MMR) as the source of heat for the hot fluids. Oil fields more proximal to the MMR have the highest temperatures of homogenization in this study, and those more distal display lower homogenization temperatures. High salinities (up to 49.4 wt. % NaCl equiv.) are observed in included fluids in carbonate cements in the south-central Michigan Basin. These values are equal to or higher than salt concentrations in the surrounding region. The only source of salt that can be identified in the Michigan Basin is the Silurian Salina Group evaporites. Lower eutectic temperatures are observed in oil fields proximal to the MMR (as low as -112º C) with a trend of higher eutectic temperatures distal from the rift (average -64º C in westernmost fields within the study area). While Salina Group evaporites are the predominant source of salt in oil fields in this study, the MMR may have provided additional cations resulting in complex fluid chemistries.

Fluids that precipitated carbonate cements in TBR oil fields likely have similar sources and timing. However, water-rock interactions along independent fault pathways modified source waters from their original compositions, giving each oil field its own unique signature. Underlying basement faults across the study area allowed fluids to move through rock simultaneously. Some fluids may have been shared where underlying fault systems are connected such as in in the Scipio, Albion, and Napoleon oil fields where similar, but not identical, CL stratigraphies are observed in dolomite cements.

A combination of density driven flow, thermal heating events, and structural pumping from reactivated basement faults likely combined to create convective fluid flow in each fault-fracture system. Data in the Basin do not directly correlate to one orogenic event, and reactivation of basement faulting driving fluid movement likely continued during inter-orogenic periods.

CHAPTER V

FUTURE WORK

The fluids observed in this study open questions for future research. Are these high temperature fluids unique to oil fields in the south-central portions of the Basin? Are these high salinity fluids unique to oil fields in the south-central portions of the Basin? Do chlorine/bromine ratios support salt sourcing from the Salina Group? Do the observed decreasing trends in salinity and temperatures exist for all directions away from the Michigan Basin? Do the observed decreasing trends in salinity and temperatures exist for all directions away from the Mid-Michigan Rift? How much influence did regional orogenies have on fluid evolution in the Michigan Basin? Future work should be undertaken to answer these questions and better understand the complex fluid history of the Michigan Basin.

Table 5: Calculated equilibrium $\delta^{18}O$ values of cement precipitating fluids. Values for equilibrium waters were calculated for dolomite cements using Matthews and Katz (1977) and for calcite cements and host limestone (LS) using Northrop and O'Neil (1969). Expected $\delta^{18}O$ values for limestones deposited from dolomite equilibrium fluids ("from same water") were calculated utilizing the same homogenization temperatures. Fluids in equilibrium with host limestone have been calculated for expected surface deposition temperature. Host limestone $\delta^{18}O$ value is an average of 5 host limestone isotope values measured in this study from Freedom and Albion oil fields (see Table 3). All $\delta^{18}O$ values are in per mil (‰).

Sample	Field	Lithology	$\delta^{18}O_{sample}$ VPDB	$\delta^{18}O_{sample}$ VSMOW	T_h °C	$\delta^{18}O_{cement}$ depositing water VSMOW	$\delta^{18}O_{limestone\ from\ same\ water}$ VPDB
127-2	Freedom	Dolomite Cement	-7.90	22.8	91 to 183	+2.3 to +10.9	-10.2 to -9.4
132-1	Northville	Dolomite Cement	-8.55	22.1	188 to 197	+10.6 to +11.2	-10.0
137-1	Northville	Calcite Cement	-12.46	18.1	163 to 254	+6.5 to +11.3	-12.5
137-2	Northville	Dolomite Cement	-8.37	22.3	243 to 258	+13.8 to +14.4	-9.6 to -9.5
138-2	Albion	Dolomite Cement	-8.50	22.1	147 to 240	+7.6 to + 13.5	-10.2 to -9.7
143-1	Albion	Dolomite Cement	-7.65	23.0	200 to 232	+12.3 to + 14.0	-9.0 to -8.9
144-1	Albion	Dolomite Cement	-8.15	22.5	110 to 122	+4.4 to +5.6	-10.2 to -10.1
147-2	Reading	Dolomite Cement	-6.59	24.1	113 to 176	+6.3 to +11.8	-8.6 to -8.1
B10	Scipio	Dolomite Cement	-8.35	22.3	124 to 162	+5.6 to +9.0	-10.3 to -10.0
M1	Scipio	Dolomite Cement	-8.84	21.8	153 to 168	+7.8 to +8.9	-10.5 to -10.4
P1	Branch Cty Core	Dolomite Cement	-8.16	22.5	123 to 162	+5.7 to +9.2	-10.1 to -9.8
P6	Branch Cty Core	Dolomite Cement	-7.27	23.4	79 to 130	+1.3 to +7.3	-9.7 to -9.1
W1	Napoleon	Dolomite Cement	-8.07	22.6	95 to 213	+2.6 to +12.6	-10.3 to -9.4
W15	Napoleon	Dolomite Cement	-8.09	22.6	114 to 144	+4.9 to +7.8	-10.1 to -9.8
Host LS Avg	-	Host Limestone	-6.31	24.4	20	-5.5	-

Table 6: Pressure Corrected Temperatures at Late Silurian Burial. Pressure-corrected temperatures of entrapment for assemblages in this study. Corrections made for estimated depth and pressures for cement emplacement during latest Silurian. Values calculated assume 0.5 km depth of burial at time of entrapment and an average lithostatic gradient of 23 MPa/km. Calculation from Zhang and Frantz (1987).

Sample	Field	Chip	Assemblage	% wt. NaCl	T_h (° C)	Corrected Temperature (° C)
86-143	Albion	1	1	35.5	207	212
86-144	Albion	1	1	30.2	121	126
86-144	Albion	2	1	25.7	113	118
86-138	Albion	1	1	25.3	228	233
86-138	Albion	2	1	27.6	189	195
86-127	Freedom	1	2	34.4	110	115
86-127	Freedom	3	1	31.6	127	132
86-127	Freedom	4	1	31.2	183	189
86-127	Freedom	5	1	30.0	113	118
WB 4066	Napoleon	1a	1	36.3	208	213
WB 4066	Napoleon	1b	1	31.2	103	108
WB 4277	Napoleon	1	1	28.1	129	134
WB 4277	Napoleon	2	1	35.7	128	133
WB 4277	Napoleon	3a	1	27.6	125	130
WB 4277	Napoleon	3b	2	33.5	134	139
86-137	Northville	8	1	34.6	250	255
86-137	Northville	2	1	32.5	246	250
86-137	Northville	3	1	26.0	188	194
86-137	Northville	4a	1	24.8	218	223
86-137	Northville	4b	2	24.5	232	238
86-137	Northville	1	1	25.9	200	206
86-147	Reading	1	1	16.4	121	127
86-147	Reading	2	1	18.7	168	173
86-147	Reading	3	1	22.1	124	130
B3854	Scipio	1a	1	29.4	133	138
B3854	Scipio	1c	3	31.6	155	160
B3854	Scipio	3	1	28.0	146	152
P3291	Wildcat	1	1	24.3	125	131
P3291	Wildcat	2	1	26.0	114	119
P3271	Wildcat	1	1	26.4	125	130
P3271	Wildcat	1	2	26.1	160	166

Table 7: Pressure Corrected Temperatures at Maximum Burial. Pressure-corrected temperatures of entrapment for assemblages in this study. Corrections made for estimated depth and pressures for cement emplacement at maximum burial; approximately early Permian. Values calculated assume 2 km depth of burial at time of entrapment and an average lithostatic gradient of 23 MPa/km. Calculation from Zhang and Frantz (1987).

Sample	Field	Chip	Assemblage	% wt.	T_h (° C)	Corrected
86-143	Albion	1	1	35.5	207	231
86-144	Albion	1	1	30.2	121	142
86-144	Albion	2	1	25.7	113	133
86-138	Albion	1	1	25.3	228	254
86-138	Albion	2	1	27.6	189	213
86-127	Freedom	1	2	34.4	110	130
86-127	Freedom	3	1	31.6	127	148
86-127	Freedom	4	1	31.2	183	206
86-127	Freedom	5	1	30.0	113	134
WB 4066	Napoleon	1a	1	36.3	208	232
WB 4066	Napoleon	1b	1	31.2	103	123
WB 4277	Napoleon	1	1	28.1	129	150
WB 4277	Napoleon	2	1	35.7	128	149
WB 4277	Napoleon	3a	1	27.6	125	146
WB 4277	Napoleon	3b	2	33.5	134	155
86-137	Northville	8	1	34.6	250	276
86-137	Northville	2	1	32.5	246	271
86-137	Northville	3	1	26.0	188	212
86-137	Northville	4a	1	24.8	218	243
86-137	Northville	4b	2	24.5	232	259
86-137	Northville	1	1	25.9	200	225
86-147	Reading	1	1	16.4	121	143
86-147	Reading	2	1	18.7	168	191
86-147	Reading	3	1	22.1	124	146
B3854	Scipio	1a	1	29.4	133	154
B3854	Scipio	1c	3	31.6	155	177
B3854	Scipio	3	1	28.0	146	168
P3291	Wildcat	1	1	24.3	125	146
P3291	Wildcat	2	1	26.0	114	135
P3271	Wildcat	1	1	26.4	125	146
P3271	Wildcat	1	2	26.1	160	183

REFERENCES

Ahern, J. L., and Panayes J. D., 1989, Evolution of the lithosphere beneath the Michigan Basin, Earth and Planetary Science Letters v. 95, no. 1-2, p. 73-84.

Allan, J. R., and Wiggins, W. D., 1993, Dolomite Reservoirs: Geochemical Techniques for Evaluating Origin and Distribution, American Association of Petroleum Geologists, 110p.

Allen, P.A., and Allen, J.R., 2013, Basin analysis: Principles and application to petroleum play assessment, 3rd edition, Chinchester, John Wiley & Sons, 619p.

Bethke, C.M., 1986, Hydrologic constraints on the genesis of the Upper Mississippi Valley mineral district from Illinois basin brines, Economic Geology v. 81, no. 2, p. 233-249.

Bodnar, R.J., 2003, Introduction to aqueous-electrolyte fluid inclusions, in Samson, I., Anderson, A. and Marshall, D.D. eds., Fluid inclusions: analysis and interpretation, Mineralogical Association of Canada, v. 32, p. 81-100.

Bodnar, R.J. and Samson, I., 2003, Introduction to fluid inclusions, in Samson, I., Anderson, A., and Marshall, D.D., eds., Fluid inclusions: analysis and interpretation, Mineralogical Association of Canada, v. 32, p. 1-8

Bodnar, RJ., and Vitnyk, M.A., 1994, Interpretation of microthermometric data for NaCI-H_2O fluid inclusions, in De Vivo, B., and Frezzotti, M.L., eds., Fluid inclusions in minerals: Methods and applications, Short course of the working group (IMA) Inclusions in Minerals, p. 117-131.

Budai, J. M., and Wilson, J. L., 1991, Diagenetic history of the Trenton and Black River formations in the Michigan Basin, in Catacosinos, P. A., and Daniels, P. A. Jr., eds., Early sedimentary evolution of the Michigan Basin: Geological Society of America Special Paper no. 256, p. 73-88.

Catacosinos, P.A., 1973, Cambrian lithostratigraphy of Michigan basin, AAPG Bulletin v. 57, no. 12, p. 2404-2418.

Catacosinos, P.A., and Daniels, P.A., eds., 1991, Early sedimentary evolution of the Michigan Basin, v. 256, Geological Society of America 248p.

Catacosinos, P.A., Daniels, P.A. Jr., and Harrison, W. B. III, 1990, Structure, Stratigraphy, and Petroleum Geology of the Michigan Basin: Chapter 30: Part II, in Selected Analog Interior Cratonic Basins: Analog Basin, p. 561-601.

Catacosinos, P.A., Daniels, P.A. Jr., and Harrison, W. B. III, 1991, Structure, stratigraphy, and petroleum geology of the Michigan Basin, Interior cratonic basins: AAPG Memoir v. 51, p. 561-601.

Cercone, K.R., 1984, Thermal history of Michigan basin, AAPG Bulletin, v. 68, no. 2, p.130-136.

Coniglio, M., Sherlock, R., Williams-Jones, A.E., Middleton, K., Frape, S. K., Purser, B., Tucker, M., and D. Zenger, 1994, Burial and hydrothermal diagenesis of Ordovician carbonates from the Michigan Basin, Ontario, Canada, in Purser, B., Tucker, M., and Zenger, D., eds., Dolomites—A volume in honour of Dolomieu, International Association of Sedimentologists, Special Publication v. 21, p. 231-254.

Coniglio, M., and Williams-Jones, A. E., 1992, Diagenesis of Ordovician carbonates from the north-east Michigan Basin, Manitoulin Island area, Ontario: evidence from petrography, stable isotopes and fluid inclusions, Sedimentology v. 39, no. 5, p. 813-836.

Cox, K., 2015, Anomalous Thermal Indicators from Authigenic Minerals in Upper Paleozoic Strata of the Michigan Basin, M.S. Thesis, no. 594, Kalamazoo, Michigan, https://scholarworks.wmich.edu/masters_theses/594.

Davies, G.R., and Smith, L.B. Jr., 2006, Structurally controlled hydrothermal dolomite reservoir facies: an overview: AAPG Bulletin, v. 90, p. 1641-1690.

Drahovzal, J.A., Harris, D.C., Wickstrom, L.H., Walker, D., Baranoski, M.T., Keith, B., and Furer, L.C., 1992, The east continent rift basin: a new discovery, Ohio Division of Geological Survey.

Ells, G.D., 1962, Structures associated with the Albion-Scipio oil field trend, Michigan Dept. of Conservation, Geological Survey Division.

Ettensohn, F.R.R., 2004. Modeling the nature and development of major Paleozoic clastic wedges in the Appalachian Basin, USA. Journal of Geodynamics, v. 37, no. 3-5, p. 657–681.

Everham, W.D., 2004, Thermal history of the Michigan basin, Houghton, Michigan Technological University, Ph.D. dissertation, 251p.

Fara, D.R., and Keith, B.D., 1988, Depositional facies and diagenetic history of the Trenton limestone in northern Indiana: Chapter 17, in Keith, B.D., ed., The Trenton Group (upper Ordovician series) of eastern North America, p. 277-298.

Fisher, J.H., Barratt, M.W., Droste, J.B., and Shaver, R.H., 1988, Michigan basin, in Sloss, L.L. ed., The Geology of North America, v. 2, p. 361-382.

Garven, G., 1995, Continental-scale groundwater flow and geologic processes, Annual Review of Earth and Planetary Sciences, v. 23, no. 1, p. 89-117.

Garven, G., and Raffensperger, J.P., 1997, Hydrogeology and geochemistry of ore genesis in sedimentary basins, in Barnes, H.L., ed., Geochemistry of hydrothermal ore deposits 3, p. 125-189.

Gautier, D.L., Dolton, G.L., Takahashi, K.I., and Varnes, K.L., 1995, National assessment of United States oil and gas resources: Results, methodology, and supporting data, No. 30, Geological Survey (US).

Girard, J.P., and Barnes, D.A., 1995, Illitization and paleothermal regimes in the Middle Ordovician St. Peter Sandstone, central Michigan basin: K-Ar, oxygen isotope, and fluid inclusion data, AAPG Bulletin, v. 79, no. 1, p. 49-69.

Goddéris, Y., François, L.M., and Veizer, J., 2001, The early Paleozoic carbon cycle, Earth and Planetary Science Letters, v. 190, no. 3-4, p. 181-196.

Goldstein, R. H., 2003, Petrographic analysis of fluid inclusions, in Samson, I., Anderson, A., and Marshall, D., eds., Fluid Inclusions: Analysis and Interpretation, Mineral Association Canada, short course 32, p. 9-53.

Goldstein, R. H., and Reynolds, T. J., 1994, Fluid inclusion microthermometry, in Goldstein, H.R., Systematics of fluid inclusions in diagenetic minerals, SEPM short course, no. 31, 199 p.

Grammer, G.M. and Harrison, W.B., 2013, Evaluation and modeling of stratigraphic control on the distribution of hydrothermal dolomite away from major fault planes, RPSEA (Research Partnership to Secure Energy for America) Final Technical Report, No. 08123.12, 997 p.

Granath V.C., 1991, Geochemical constraints on the origin of dolomite in the Ordovician Trenton and Black River limestones, Albion-Scipio area, Michigan, AAPG Bulletin, v. 75, CONF-910403.

Gregg, J. M., 1982, The origin of xenotopic dolomite texture, East Lansing, Michigan State University, unpublished Ph.D. dissertation, 151 p.

Gregg, J.M., and Sibley, D.F., 1984, Epigenetic dolomitization and the origin of xenotopic dolomite texture, Journal of Sedimentary Petrology, v. 54, no. 3, p. 908-931.

Gregg, J.M., and Shelton, K.L., 2012, Mississippi Valley-type mineralization and ore deposits in the Cambrian–Ordovician great American carbonate bank, in Derby, J.R., Fritz, R.D., Longacre, S.A., Morgan, W.A., and Sternbach, C.A., eds., The great American carbonate bank: The geology and economic resources of the Cambrian–Ordovician Sauk megasequence of Laurentia, AAPG Memoir 98, p. 161-185.

Haefner, R.J., 1986, Mississippi Valley Type Mineralization and Dolomitization of the Trenton Limestone, Wyandot County, Ohio, Ph.D. dissertation, Bowling Green State University, Bowling Green, Ohio.

Haefner, R.J., Mancuso, J.J., Frizado, J.P., Shelton, K.L., and Gregg, J.M., 1988, Crystallization temperatures and stable isotope compositions of Mississippi Valley-type carbonates and sulfides of the Trenton Limestone, Wyandot County, Ohio, Economic Geology, v. 83, p. 1061-1069.

Haeri-Ardakani, O., Al-Aasm, I., and Coniglio, M., 2013, Fracture mineralization and fluid flow evolution: an example from Ordovician–Devonian carbonates, southwestern Ontario, Canada, Geofluids, v. 13, no. 1, p. 1-20.

Hall, W.E., and Friedman, I., 1963, Composition of fluid inclusions, Cave-in-Rock fluorite district, Illinois, and Upper Mississippi Valley zinc-lead district, Economic Geology, v. 58, no. 6, p. 886-911.

Haroldson, E.L., Brown, P.E., and Bodnar, R.J., 2018, Involvement of variably-sourced fluids during the formation and later overprinting of Paleoproterozoic Au-Cu mineralization: Insights gained from a fluid inclusion assemblage approach, Chemical Geology, v. 497, p. 115-127.

Hinze, W.J., Kellogg, R.L., and O'Hara, N.W., 1975, Geophysical studies of basement geology of southern peninsula of Michigan, AAPG Bulletin v. 59, no. 9, p. 1562-1584.

Hobbs, M.Y., Frape, S.K., Shouakar-Stash, O., and Kennell, L.R., 2011, Regional hydrogeochemistry–southern Ontario, Nuclear Waste Management Organization Report 157.

Howell, P.D., and Van Der Pluijm, B.A., 1990, Early history of the Michigan basin: Subsidence and Appalachian tectonics, Geology, v. 18, no. 12, p. 1195-1198.

Howell, P.D., and Van Der Pluijm, B.A., 1999, Structural sequences and styles of subsidence in the Michigan basin, Geological Society of America Bulletin, v. 111, no. 7, p. 974-991.

Hurley, N. F., and Budros, R., 1990, Albion-Scipio and Stoney Point Fields – U.S.A. Michigan Basin, in Beaumont, E.A., and Foster, N.H., eds., Stratigraphic Traps I: AAPG Treatise of Petroleum Geology, Atlas of Oil and Gas Fields, p. 1-37.

Jaiswal, P., Gregg, J.M., Parks, S., Holman, R., Mohammadi, S. and Grammer, G.M., 2019, Evidence of fault/fracture "Hydrothermal" reservoirs in the southern midcontinent Mississippian carbonates, in Grammer, G.M., Gregg, J.M., Puckette, J.O., Jaiswal, P., Mazzullo, S.J., Pranter, M.J., and Goldstein, R.H., eds., Mississippian Reservoirs of the Midcontinent, AAPG Memoir 116, DOI:10.1306/13632161M1163366.

Johnson, A.W., Shelton, K.L., Gregg, J.M., Somerville, I.D., wright, W.R., and Nagy, Z.R., 2009, Regional studies of dolomites and their included fluids: recognizing multiple chemically distinct fluids during the complex diagenetic history of Lower Carboniferous (Mississippian) rocks of the Irish Zn-Pb ore field: Mineralogy and Petrology, v. 96, p. 1–18.

Land, L.S., 1980, The isotopic and trace element geochemistry of dolomite: the state of the art, SEPM Special Publication, no. 28, p. 87-110.

Lilienthal, R.T., 1978, Stratigraphic cross-sections of the Michigan Basin, Geological Survey Division Michigan Department of Natural Resources.

Luczaj, J.A., 2001, Epigenetic dolomitization and sulfide mineralization in Paleozoic rocks of eastern Wisconsin: Implications for fluid flow out of the Michigan Basin, USA, Ph.D. dissertation, John Hopkins University, Baltimore, Maryland, 443 p.

Luczaj, J.A., Harrison, W.B., III, and Williams, N.S., 2006, Fractured hydrothermal dolomite reservoirs in the Devonian Dundee Formation of the central Michigan Basin, AAPG bulletin, v. 90, no. 11, p. 1787-1801.

Machel, H.G., 1985, Cathodoluminescence in Calcite and Dolomite and Its Chemical Interpretation, *Geoscience* Canada, v. 12, no. 4, p. 139-147.

Machel, H.G., and Lonnee, J., 2002, Hydrothermal dolomite—A product of poor definition and imagination, Sedimentary geology, v. 152, no. 3-4, p. 163-171.

Matthews, A., and Katz, A., 1977, Oxygen isotope fractionation during the dolomitization of calcium carbonate, Geochimica et Cosmochimica Acta, v. 41, no. 10, p.1431-1438.

McCaig, A.M., Wayne, D.M. and Rosenbaum, J.M., 2000. Fluid expulsion and dilatancy pumping during thrusting in the Pyrenees: Pb and Sr isotope evidence, Geological Society of America Bulletin, v. 112, no. 8, p. 1199-1208.

McNutt, R. H., Frape, S.K., and Dollar, P., 1987, A strontium, oxygen and hydrogen isotopic composition of brines, Michigan and Appalachian Basins, Ontario and Michigan, Applied Geochemistry, v. 2, no. 5-6, p. 495-505.

Moyer, R.B., 1982, Thermal maturity and organic content of selected Paleozoic formations—Michigan Basin: unpublished M.S. thesis, East Lansing, Michigan State University, 62 p.

Muir-Wood, R., and King, G.C., 1993, Hydrological signatures of earthquake strain, Journal of Geophysical Research: Solid Earth, v. 98, no. B12, p. 22035-22068.

Nunn, J.A., Sleep, N.H., and Moore, W.E., 1984, Thermal subsidence and generation of hydrocarbons in Michigan Basin, AAPG bulletin, v. 68 no. 3, p. 296-315.

Nurkhanuly, U., 2012, Structurally controlled hydrothermal dolomite, Eganville-Douglas Paleozoic outlier, Ottawa-Bonnechere graben, eastern Ontario, unpublished Ph.D. dissertation, Ottowa, Carleton University, 98 p.

O'Neil, J.R., Clayton, R.N., and Mayeda, T.K., 1969, Oxygen isotope fractionation in divalent metal carbonates, The Journal of Chemical Physics, v. 51, no. 12, p. 5547-5558.

Patchen, D.G., Hickman, J.B., Harris, D.C., Drahovzal, J.A., Lake, P.D., Smith, L.B., Nyahay, R., Schulze, R., Riley, R.A., Baranoski, M.T. and Wickstrom, L.H., 2006, A geologic play book for Trenton-Black River Appalachian basin exploration: US Department of Energy Report, Morgantown, West Virginia, DOE Award Number DE-FC26-03NT41856.

Person, M., and Garven, G., 1992, Hydrologic constraints on petroleum generation within continental rift basins: Theory and application to the Rhine Graben, AAPG Bulletin, v. 76, p. 468–488.

Prouty, C.E., 1988, Trenton Exploration and Wrenching Tectonics in Michigan Basin and Environs, in Keith, B.D., ed., The Trenton Group (upper Ordovician series) of eastern North America p. 207-236.

Qing, H. and Veizer, J., 1994, Oxygen and carbon isotopic composition of Ordovician brachiopods: Implications for coeval seawater, Geochimica et Cosmochimica Acta, v. 58, no. 20, p. 4429-4442.

Qing, H., Barnes, C.R., Buhl, D. and Veizer, J., 1998, The strontium isotopic composition of Ordovician and Silurian brachiopods and conodonts: relationships to geological events and implications for coeval seawater, Geochimica et Cosmochimica Acta, v. 62, no. 10, p.1721-1733.

Reed, J.D., Illich, H.A. and Horsfield, B., 1986, Biochemical evolutionary significance of Ordovician oils and their sources, Organic Geochemistry, v. 10, no. 1-3, p. 347-358.

Sagan, J.A. and Hart, B.S., 2006. Three-dimensional seismic-based definition of fault-related porosity development: Trenton–Black River interval, Saybrook, Ohio, AAPG bulletin, v. 90, no. 11, p. 1763-1785.

Shelton, K.L., Hendry, J.P., Gregg, J.M., Truesdale, J.P., and Somerville, I.D., 2019, Fluid circulation and fault-fracture – related diagenesis in Mississippian syn-rift carbonate rocks on the northeast margin of the metaliferous Dublin Basin, Ireland: Journal of Sedimentary Research, in press, DOI: http://dx.doi.org/10.2110/jsr.2019.31.

Shields, G.A., Carden, G.A., Veizer, J., Meidla, T., Rong, J.Y. and Li, R.Y., 2003, Sr, C, and O isotope geochemistry of Ordovician brachiopods: A major isotopic event around the Middle-Late Ordovician transition, Geochimica et Cosmochimica Acta, v. 67, no. 11, p. 2005-2025.

Sibley, D.F., and Gregg, J.M., 1987, Classification of dolomite rock textures, Journal of Sedimentary Petrology v. 57, no. 6, p. 967-975.

Sleep, N.H., Sloss, L.L., Bally, A.W. and Bender, P.L., 1980, The Michigan Basin, Dynamics of plate interiors, v. 1, p. 93-98.

Sloss, L.L., 1963, Sequences in the cratonic interior of North America, Geological Society of America Bulletin, v. 75, p. 93–113.

Smith, L.B. Jr., 2006, Origin and reservoir characteristics of Upper Ordovician Trenton–Black River hydrothermal dolomite reservoirs in New York, AAPG bulletin, v. 90, no. 11, p. 1691-1718.

Taylor, T.R. and Sibley, D.F., 1986, Petrographic and geochemical characteristics of dolomite types and the origin of ferroan dolomite in the Trenton Formation, Ordovician, Michigan Basin, USA, Sedimentology, v. 33, no.1, p. 61-86.

Van Schmus, W.R. and Hinze, W.J., 1985, The midcontinent rift system, Annual Review of Earth and Planetary Sciences, v. 13, no. 1, p. 345-383.

Veizer, J., Ala, D., Azmy, K., Bruckschen, P., Buhl, D., Bruhn, F., Carden, G.A., Diener, A., Ebneth, S., Godderis, Y. and Jasper, T., 1999, $^{87}Sr/^{86}Sr$, $\delta^{13}C$ and $\delta^{18}O$ evolution of Phanerozoic seawater, Chemical geology, v. 161, no. 1-3, p. 59-88.

Versical, R. T., 1991, Basement control on the development of selected Michigan Basin oil and gas fields as constrained by fabric elements in Paleozoic limestones: unpublished M.S. thesis, Kalamazoo, Western Michigan University, 200 p.

Voss, R.L., Hagni, R.D., and Gregg, J.M., 1989, Sequential deposition of zoned dolomite and its relationship to sulfide mineral paragenetic sequence in the Viburnum Trend, southeast Missouri, Carbonates and evaporites v. 4, no. 2, p. 195-209.

Vugrinovich, R., 1988, Relationships between regional hydrogeology and hydrocarbon occurrences in Michigan, USA, Journal of petroleum geology, v. 11, no. 4, p. 429-442.

Wendte, J., Chi, G., Al-Aasm, I. and Sargent, D., 2009, Fault/fracture controlled hydrothermal dolomitization and associated diagenesis of the Upper Devonian Jean Marie Member (Redknife Formation) in the July Lake area of northeastern British Columbia, Bulletin of Canadian Petroleum Geology, v. 57, no. 3, p. 275-322.

Wilkinson, J.J., Bodnar, R. and Cline, J., 2010, A review of fluid inclusion constraints on mineralization in the Irish ore field and implications for the genesis of sediment-hosted Zn-Pb deposits, Economic Geology and the Bulletin of the Society of Economic Geologists, v. 105, no 2, p. 417–442.

Wilkinson, J.J., Eyre, S.L. and Boyce, A.J., 2005, Ore-forming processes in Irish-type carbonate-hosted Zn-Pb deposits: Evidence from mineralogy, chemistry, and isotopic composition of sulfides at the Lisheen mine, Economic Geology, v. 100, no. 1, p. 63-86.

Wilson, J.L., Budai, J.M., and Sengupta, A., 2001, Trenton-Black River formations of Michigan basin, Masera Corporation, Tulsa, Oklahoma, Search and Discovery Article, 10020.

Yoo, C. M., Gregg, J. M., and Shelton, K. L., 2000, Dolomitization and dolomite neomorphism: Trenton and Black River limestones (Middle Ordovician) Northern Indiana, U.S.A., Journal of Sedimentary Research, v. 70, p. 265-274.

Zhang, Y.G., and Frantz, J.D., 1987, Determination of the homogenization temperatures and densities of supercritical fluids in the system NaCl-KCl-$CaCl_2$-H_2O using synthetic fluid inclusions, Chemical Geology, v. 64, no. 3, p. 335–350.

APPENDICES

Table 1: Fluid Inclusion Master Data Table. Thin lines separate assemblages. Abbreviations are as follows: Sample Identifier (Sample ID), well location in section-township-range (S-T-R), Depths in meters (m), Chip number (#), Fluid inclusion assemblage number (Assmb #), Fluid inclusion number (Flinc #), homogenization temperature (T_h), last ice melt temperatures (T_m), first ice melts interpreted as eutectic temperatures (T_e), equivalent fluid salinity in wt. % NaCl (NaCl Eqiv) (equitation of Bodnar and Vitnyk, 1994), average homogenization temperature for the assemblage (Avg-T_h), average salinity for the assemblage in wt. % NaCl (Avg-NaCl), fluid inclusion type (Flinc Type), mineral (Minl), dolomite (d), calcite (c). In the lab notes, heating runs refer to raising temperatures from ~20º C to homogenization temperatures (100º C or more), freezing runs refer to lowering temperatures from ~20º C to temperatures well below 0º C (-150º C or more) to fully freeze the sample prior to attempts to record last ice melt temperatures, melting runs refer to raising temperatures from well below 0º C after freezing runs to record eutectic and last ice melt temperatures, hydrocarbon (HC).

Sample ID	Well Name	S-T-R	Depth (m)	Field	County	Chip #	Assmb #	Flinc #	T_h	T_m	NaCl Eqiv	Avg-T_h	Avg-NaCl	Flinc Type	Minl	Lab Notes
86-143	Humble Riley #2	26-3S-4W	1299.1	Albion	Calhoun	1	1	1	232	-39.5	35.7	207	35.5		d	
86-143	Humble Riley #2	26-3S-4W	1299.1	Albion	Calhoun	1	1	2	203						d	
86-143	Humble Riley #2	26-3S-4W	1299.1	Albion	Calhoun	1	1	3	200						d	
86-143	Humble Riley #2	26-3S-4W	1299.1	Albion	Calhoun	1	1	4	204	-39	35.2				d	
86-143	Humble Riley #2	26-3S-4W	1299.1	Albion	Calhoun	1	1	5	203						d	
86-143	Humble Riley #2	26-3S-4W	1299.1	Albion	Calhoun	1	1	6	201						d	
86-143	Humble Riley #2	26-3S-4W	1299.1	Albion	Calhoun	1	1	7	203						do	
86-144	Humble-Hartung #1	1-4S-4W	1239.3	Albion	Calhoun	1	1	1	120	-32.0	30.0	121.1	30.2	P	d	Not fluorescent but near proximity to white/pale yellow fluorescing inclusions
86-144	Humble-Hartung #1	1-4S-4W	1239.3	Albion	Calhoun	1	1	2	122	-31.8	29.8			P	d	Not fluorescent but near proximity to white/pale yellow fluorescing inclusions
86-144	Humble-Hartung #1	1-4S-4W	1239.3	Albion	Calhoun	1	1	3	121	-33.5	31.0			P	d	Not fluorescent but near proximity to white/pale yellow fluorescing inclusions
86-144	Humble-Hartung #1	1-4S-4W	1239.3	Albion	Calhoun	2	1	1	114	-23.0	24.3	113.0	25.7		d	High confidence in measurements
86-144	Humble-Hartung #1	1-4S-4W	1239.3	Albion	Calhoun	2	1	2	111	-28.0	27.4				d	
86-144	Humble-Hartung #1	1-4S-4W	1239.3	Albion	Calhoun	2	1	3	111	-26.4	26.4				d	
86-144	Humble-Hartung #1	1-4S-4W	1239.3	Albion	Calhoun	2	1	4	119	-23.4	24.6				d	High confidence in measurements
86-144	Humble-Hartung #1	1-4S-4W	1239.3	Albion	Calhoun	2	1	5	110						d	Too dark to see ice melt
86-138	Humble-Kryst Comm #1	7-4S-3W	1210.4	Albion	Jackson	1	1	1	201	-21.4	23.3	227.9	25.3		d	
86-138	Humble-Kryst Comm #1	7-4S-3W	1210.4	Albion	Jackson	1	1	2	221	-26.0	26.2				d	
86-138	Humble-Kryst Comm #1	7-4S-3W	1210.4	Albion	Jackson	1	1	3	238	-25.6	25.9				d	
86-138	Humble-Kryst Comm #1	7-4S-3W	1210.4	Albion	Jackson	1	1	4	240	-25.1	25.6				d	

86-138	Humble-Kryst Comm #1	7-4S-3W	1210.4	Albion	Jackson	1	1	5	240	-24.7	25.4				d	
86-138	Humble-Kryst Comm #1	7-4S-3W	1210.4	Albion	Jackson	2	1	1	230	-26.0	26.2	188.7	27.6	P		High confidence in measurements
86-138	Humble-Kryst Comm #1	7-4S-3W	1210.4	Albion	Jackson	2	1	2	148	-27.4	27.0			P	d	
86-138	Humble-Kryst Comm #1	7-4S-3W	1210.4	Albion	Jackson	2	1	3	147	-29.8	28.5			P	d	
86-138	Humble-Kryst Comm #1	7-4S-3W	1210.4	Albion	Jackson	2	1	4	230	-30.0	28.7			P	d	
86-127	Buss Haab #1	8-3S-4E	1313.7	Freedom	Washtenaw	1	1	1	117			113.3		P	d	Appears to have leaked after first heating
86-127	Buss Haab #1	8-3S-4E	1313.7	Freedom	Washtenaw	1	1	2	119					P	d	
86-127	Buss Haab #1	8-3S-4E	1313.7	Freedom	Washtenaw	1	1	3						P	d	Bubble moved at -54, possible Te
86-127	Buss Haab #1	8-3S-4E	1313.7	Freedom	Washtenaw	1	1	4	97					P	d	
86-127	Buss Haab #1	8-3S-4E	1313.7	Freedom	Washtenaw	1	1	5	110					P	d	
86-127	Buss Haab #1	8-3S-4E	1313.7	Freedom	Washtenaw	1	1	6	117					P	d	
86-127	Buss Haab #1	8-3S-4E	1313.7	Freedom	Washtenaw	1	1	7	114					P	d	
86-127	Buss Haab #1	8-3S-4E	1313.7	Freedom	Washtenaw	1	1	8	119					P	d	
86-127	Buss Haab #1	8-3S-4E	1313.7	Freedom	Washtenaw	1	2	1	95			109.7	34.4	P	d	
86-127	Buss Haab #1	8-3S-4E	1313.7	Freedom	Washtenaw	1	2	2	124	-36.9	33.5			P	d	
86-127	Buss Haab #1	8-3S-4E	1313.7	Freedom	Washtenaw	1	2	3	111	-38.7	35.0			P	d	
86-127	Buss Haab #1	8-3S-4E	1313.7	Freedom	Washtenaw	1	2	4	108	-37.3	33.8			P	d	
86-127	Buss Haab #1	8-3S-4E	1313.7	Freedom	Washtenaw	1	2	5	111	-38.9	35.1			P	d	
86-127	Buss Haab #1	8-3S-4E	1313.7	Freedom	Washtenaw	3	1	1	155			127.1	31.6	P	d	
86-127	Buss Haab #1	8-3S-4E	1313.7	Freedom	Washtenaw	3	1	2	139					P	d	
86-127	Buss Haab #1	8-3S-4E	1313.7	Freedom	Washtenaw	3	1	3	142					P	d	
86-127	Buss Haab #1	8-3S-4E	1313.7	Freedom	Washtenaw	3	1	4	136					P	d	

86-127	Buss Haab #1	8-3S-4E	1313.7	Freedom	Washtenaw	3	1	5	126					P	d	
86-127	Buss Haab #1	8-3S-4E	1313.7	Freedom	Washtenaw	3	1	6	94					P	d	
86-127	Buss Haab #1	8-3S-4E	1313.7	Freedom	Washtenaw	3	1	7	133					P	d	
86-127	Buss Haab #1	8-3S-4E	1313.7	Freedom	Washtenaw	3	1	8	91	-35.0	-50	32.0		P	d	
86-127	Buss Haab #1	8-3S-4E	1313.7	Freedom	Washtenaw	4	1	1	>200	-33.8		31.2	183.0 31.2	P	d	
86-127	Buss Haab #1	8-3S-4E	1313.7	Freedom	Washtenaw	4	1	4	183					P	d	Only inclusion to appear not stretched after first heating run
86-127	Buss Haab #1	8-3S-4E	1313.7	Freedom	Washtenaw	5	1	1	114	-32.0		30.0	113.3 30.0	P	d	High confidence in measurements
86-127	Buss Haab #1	8-3S-4E	1313.7	Freedom	Washtenaw	5	1	2	114					P	d	High confidence in measurements
86-127	Buss Haab #1	8-3S-4E	1313.7	Freedom	Washtenaw	5	1	3	106	-32.0		30.0		P	d	High confidence in measurements
86-127	Buss Haab #1	8-3S-4E	1313.7	Freedom	Washtenaw	5	1	4						P	d	High confidence in measurements
86-127	Buss Haab #1	8-3S-4E	1313.7	Freedom	Washtenaw	5	1	5	114	-32.2		30.1		P	d	High confidence in measurements
86-127	Buss Haab #1	8-3S-4E	1313.7	Freedom	Washtenaw	5	1	6	114					P	d	High confidence in measurements
86-127	Buss Haab #1	8-3S-4E	1313.7	Freedom	Washtenaw	5	1	7	116	-32.0		30.0		P	d	High confidence in measurements
86-127	Buss Haab #1	8-3S-4E	1313.7	Freedom	Washtenaw	5	1	8	114					P	d	High confidence in measurements
86-127	Buss Haab #1	8-3S-4E	1313.7	Freedom	Washtenaw	5	1	9	114					P	d	High confidence in measurements
WB 4066	West Bay #1-22	21-4S-2E	1239.3	Napoleon	Jackson	1a	1	2	213				207.7 36.3		d	
WB 4066	West Bay #1-22	21-4S-2E	1239.3	Napoleon	Jackson	1a	1	4	203						d	
WB 4066	West Bay #1-22	21-4S-2E	1239.3	Napoleon	Jackson	1a	1	5	208	-40.2		36.3			d	
WB 4066	West Bay #1-22	21-4S-2E	1239.3	Napoleon	Jackson	1a	2	7	169						d	
WB 4066	West Bay #1-22	21-4S-2E	1239.3	Napoleon	Jackson	1b	1	1	95	-39.1		35.3	102.7 31.2		d	
WB 4066	West Bay #1-22	21-4S-2E	1239.3	Napoleon	Jackson	1b	1	3	110						d	
WB 4066	West Bay #1-22	21-4S-2E	1239.3	Napoleon	Jackson	1b	1	5		-28.0		27.4			d	

WB 4066	West Bay #1-22	21-4S-2E	1239.3	Napoleon	Jackson	1b	1	6		-33.4		30.9				d	
WB 4277	West Bay #1-22	21-4S-2E	1303.6	Napoleon	Jackson	1	1	1	131	-30.0	-66.5	28.7	129.3	28.6	P	d	Bubble back after freezing run 2, w/o bubble Tm = -3.5C, w bubble Tm = -30C, daughter halite nucleates when bubble is not present on melting runs, no daughter when bubble present
WB 4277	West Bay #1-22	21-4S-2E	1303.6	Napoleon	Jackson	1	1	2	116	-30.2		28.8			P	d	
WB 4277	West Bay #1-22	21-4S-2E	1303.6	Napoleon	Jackson	1	1	3	135	-30.2		28.8			P	d	
WB 4277	West Bay #1-22	21-4S-2E	1303.6	Napoleon	Jackson	1	1	4	139	-29.2		28.2			P	d	
WB 4277	West Bay #1-22	21-4S-2E	1303.6	Napoleon	Jackson	1	1	5	114	-28.3	-63	27.6		27.8	P	d	Hydrohalite nucleates during freezing runs, melts before 0C during melting
WB 4277	West Bay #1-22	21-4S-2E	1303.6	Napoleon	Jackson	1	1	6	131	-29.0		28.0			P	d	Low confidence, difficult to see
WB 4277	West Bay #1-22	21-4S-2E	1303.6	Napoleon	Jackson	1	1	7	139	-29.0		28.0			P	d	
WB 4277	West Bay #1-22	21-4S-2E	1303.6	Napoleon	Jackson	1	1	8		-27.7		27.2			P	d	
WB 4277	West Bay #1-22	21-4S-2E	1303.6	Napoleon	Jackson	1	1	9		-29.0		28.0			P	d	
WB 4277	West Bay #1-22	21-4S-2E	1303.6	Napoleon	Jackson	2	1	1	128	-41.4	-88.7	37.5	127.9	35.7	P	d	
WB 4277	West Bay #1-22	21-4S-2E	1303.6	Napoleon	Jackson	2	1	2	127	-34.0	-88.7	31.3			P	d	Bubble missing after first heating run
WB 4277	West Bay #1-22	21-4S-2E	1303.6	Napoleon	Jackson	2	1	3	129	-42.4	-88.7	38.5			P	d	
WB 4277	West Bay #1-22	21-4S-2E	1303.6	Napoleon	Jackson	3a	1	1	129	-28.3	-66.4	27.6	125.0	27.6		d	
WB 4277	West Bay #1-22	21-4S-2E	1303.6	Napoleon	Jackson	3a	1	2	124							d	
WB 4277	West Bay #1-22	21-4S-2E	1303.6	Napoleon	Jackson	3a	1	3	122							d	
WB 4277	West Bay #1-22	21-4S-2E	1303.6	Napoleon	Jackson	3a	1	4	126							d	
WB 4277	West Bay #1-22	21-4S-2E	1303.6	Napoleon	Jackson	3a	1	5	124							d	
WB 4277	West Bay #1-22	21-4S-2E	1303.6	Napoleon	Jackson	3b	2	1	144	-36.9	-68.6	33.5	133.7	33.5		d	
WB 4277	West Bay #1-22	21-4S-2E	1303.6	Napoleon	Jackson	3b	2	2	123	-37.0		33.6				d	

86-132	CPC #204	1-1S-7E	1353.0	Northville	Washtenaw	1	1	1	69			67.75	30.8	S	d	
86-132	CPC #204	1-1S-7E	1353.0	Northville	Washtenaw	1	1	2	69					S	d	
86-132	CPC #204	1-1S-7E	1353.0	Northville	Washtenaw	1	1	3	68	-33.3	30.8			S	d	
86-132	CPC #204	1-1S-7E	1353.0	Northville	Washtenaw	1	1	4	65	-33.2	30.8			S	d	
86-132	CPC #204	1-1S-7E	1353.0	Northville	Washtenaw	1	2	6	188						d	
86-132	CPC #204	1-1S-7E	1353.0	Northville	Washtenaw	1	2	7	197						d	
86-132	CPC #204	1-1S-7E	1353.0	Northville	Washtenaw	1	2	9	190						d	
86-137	CPC #204	1-1S-7E	1393.2	Northville	Washtenaw	8	1	1	258	-38.3	34.6	250.3	34.6		d	Low confidence for Tm
86-137	CPC #204	1-1S-7E	1393.2	Northville	Washtenaw	8	1	2	243						d	
86-137	CPC #204	1-1S-7E	1393.2	Northville	Washtenaw	8	1	3	248						d	
86-137	CPC #204	1-1S-7E	1393.2	Northville	Washtenaw	8	1	4	252	-112					d	
86-137	CPC #204	1-1S-7E	1393.2	Northville	Washtenaw	8	1	5		-104					d	
86-137	CPC #204	1-1S-7E	1393.2	Northville	Washtenaw	2	1	1	243	-35.4	32.3	245.5	32.5	PS	c	Multilevel, potentially healed fracture flincs
86-137	CPC #204	1-1S-7E	1393.2	Northville	Washtenaw	2	1	2	251	-37.1	33.6			PS	c	Rugose surface, potentially healed fracture flincs
86-137	CPC #204	1-1S-7E	1393.2	Northville	Washtenaw	2	1	3						PS	c	No bubble, potential daughter halite, unable to recognize ice, potentially healed fracture flincs
86-137	CPC #204	1-1S-7E	1393.2	Northville	Washtenaw	2	1	4	175	-50.8	49.4			PS	c	Bubble larger after first heating run (leaked), did not homogenize during 2nd heating, halite daughter more easily visualized after leaking, potentially healed fracture flincs
86-137	CPC #204	1-1S-7E	1393.2	Northville	Washtenaw	2	1	5	243	-34.8	31.9			PS	c	Potentially healed fracture flincs
86-137	CPC #204	1-1S-7E	1393.2	Northville	Washtenaw	2	1	6	246	-35.3	32.3			PS	c	Very rugose surface, potentially healed fracture flincs

86-137	CPC #204	1-1S-7E	1393.2	Northville	Washtenaw	3	1	1	163			188.0	26.0	PS	c	Low confidence, appears to be curved healed fracture
86-137	CPC #204	1-1S-7E	1393.2	Northville	Washtenaw	3	1	2						PS	c	May not have had a bubble or couldn't see it
86-137	CPC #204	1-1S-7E	1393.2	Northville	Washtenaw	3	1	3	196	-25.6	25.9			PS	c	Appears to be curved healed fracture
86-137	CPC #204	1-1S-7E	1393.2	Northville	Washtenaw	3	1	4	212	-25.6	25.9			PS	c	Appears to be curved healed fracture
86-137	CPC #204	1-1S-7E	1393.2	Northville	Washtenaw	3	1	5	185	-26.0	26.2			PS	c	Appears to be curved healed fracture
86-137	CPC #204	1-1S-7E	1393.2	Northville	Washtenaw	3	1	6	185	-25.5	25.9			PS	c	Appears to be curved healed fracture
86-137	CPC #204	1-1S-7E	1393.2	Northville	Washtenaw	4a	1	1	206	-19.5	22.0	217.6	24.8		c	Halite daughter present
86-137	CPC #204	1-1S-7E	1393.2	Northville	Washtenaw	4a	1	2	229	-25.8	26.1				c	
86-137	CPC #204	1-1S-7E	1393.2	Northville	Washtenaw	4a	1	3	218	-26.2	26.3				c	
86-137	CPC #204	1-1S-7E	1393.2	Northville	Washtenaw	4b	2	1	207	-11.0	15.0	232.4	24.5		c	Bubble in new position after first heating run
86-137	CPC #204	1-1S-7E	1393.2	Northville	Washtenaw	4b	2	2	228	-26.8	26.7				c	
86-137	CPC #204	1-1S-7E	1393.2	Northville	Washtenaw	4b	2	3	254	-28.1	27.5				c	Bubble moved after first heating or never came back
86-137	CPC #204	1-1S-7E	1393.2	Northville	Washtenaw	4b	2	4	241	-30.6	29.0				c	
86-137	CPC #204	1-1S-7E	1393.2	Northville	Washtenaw	1	1	1	>200	-25.5	25.9	200.0	25.9		d	Cubic Halite daughter present
86-137	CPC #204	1-1S-7E	1393.2	Northville	Washtenaw	1	1	2	>200	-25.5	25.9				d	
86-137	CPC #204	1-1S-7E	1393.2	Northville	Washtenaw	1	1	3	>200	-25.6	25.9				d	
86-137	CPC #204	1-1S-7E	1393.2	Northville	Washtenaw	1	1	4	>200	-25.8	26.1				d	
86-137	CPC #204	1-1S-7E	1393.2	Northville	Washtenaw	1	1	5	>200						d	
86-147	Anderson-Whitaker #2	29-7S-4W	965.0	Reading	Hillsdale	1	1	1	121	-12.4	16.3	121.5	16.4	P	d	High confidence in measurements, bubble returned at -30C after heating
86-147	Anderson-Whitaker #2	29-7S-4W	965.0	Reading	Hillsdale	1	1	2	122	-12.5	16.4			P	d	High confidence in measurements, bubble

																returned at 10C after heating
86-147	Anderson-Whitaker #2	29-7S-4W	965.0	Reading	Hillsdale	2	1	1	176	-15.5		19.0	167.8	18.7	P	d	
86-147	Anderson-Whitaker #2	29-7S-4W	965.0	Reading	Hillsdale	2	1	2	160	-14.6		18.3			P	d	
86-147	Anderson-Whitaker #2	29-7S-4W	965.0	Reading	Hillsdale	3	1	1		-22.0		23.7	124.5	22.1	PS	d	Bubble shrank with heating but did not run above 200 C, proportionally larger than other flinc bubbles
86-147	Anderson-Whitaker #2	29-7S-4W	965.0	Reading	Hillsdale	3	1	2	120	-20.0		22.4				d	
86-147	Anderson-Whitaker #2	29-7S-4W	965.0	Reading	Hillsdale	3	1	3	113	-20.0		22.4				d	
86-147	Anderson-Whitaker #2	29-7S-4W	965.0	Reading	Hillsdale	3	1	4	123	-13.0		16.9				d	
86-147	Anderson-Whitaker #2	29-7S-4W	965.0	Reading	Hillsdale	3	1	5	133	-24.0		25.0				d	
86-147	Anderson-Whitaker #2	29-7S-4W	965.0	Reading	Hillsdale	3	1	6	133							d	Couldn't see ice melt due to rugose shape
M3940	Mann #6	23-5S-3W	1200.9	Scipio	Hillsdale	1	1	1	166				160.6		P	d	Low confidence, never saw ice, may be HC inclusions, no fluorescence
M3940	Mann #6	23-5S-3W	1200.9	Scipio	Hillsdale	1	1	2	153		-37				P	d	Low confidence, never saw ice melt, may be HC inclusions, no fluorescence
M3940	Mann #6	23-5S-3W	1200.9	Scipio	Hillsdale	1	1	3	168						P	d	Low confidence, never saw ice, may be HC inclusions, no fluorescence, may have daughter crystal
M3940	Mann #6	23-5S-3W	1200.9	Scipio	Hillsdale	1	1	6	156						P	d	Low confidence, never saw ice, may be HC inclusions, no fluorescence
B3854	Buehrer #1	11-5S-3W	1174.7	Scipio	Hillsdale	1a	1	1	131	-31.2		29.4	132.6	29.4		d	
B3854	Buehrer #1	11-5S-3W	1174.7	Scipio	Hillsdale	1a	1	8	132							d	
B3854	Buehrer #1	11-5S-3W	1174.7	Scipio	Hillsdale	1a	1	9	135							d	
B3854	Buehrer #1	11-5S-3W	1174.7	Scipio	Hillsdale	1c	3	2	150	-35.0		32.0	155.1	31.6		d	
B3854	Buehrer #1	11-5S-3W	1174.7	Scipio	Hillsdale	1c	3	4	153	-34.5	-62	31.7				d	
B3854	Buehrer #1	11-5S-3W	1174.7	Scipio	Hillsdale	1c	3	5	162	-33.5	-62	31.0				d	

B3854	Buehrer #1	11-5S-3W	1174.7	Scipio	Hillsdale	1c	3	6	155						d		
B3854	Buehrer #1	11-5S-3W	1174.7	Scipio	Hillsdale	1b	2	1	143						d		
B3854	Buehrer #1	11-5S-3W	1174.7	Scipio	Hillsdale	1b	2	2	124						d		
B3854	Buehrer #1	11-5S-3W	1174.7	Scipio	Hillsdale	1b	2	3	149						d		
B3854	Buehrer #1	11-5S-3W	1174.7	Scipio	Hillsdale	3	1	1	138	-27.0	-63	26.8	146.3	28.0	d		
B3854	Buehrer #1	11-5S-3W	1174.7	Scipio	Hillsdale	3	1	2	158	-27.4	-65.4	27.0			d		
B3854	Buehrer #1	11-5S-3W	1174.7	Scipio	Hillsdale	3	1	4	160	-31.0		29.3			d		
B3854	Buehrer #1	11-5S-3W	1174.7	Scipio	Hillsdale	3	1	5	136	-27.2		26.9			d		
B3854	Buehrer #1	11-5S-3W	1174.7	Scipio	Hillsdale	3	1	6	140	-32.0	-57.3	30.0			d		
P3291	Arco Peck #-16	16-5S-7W	997.0	Wildcat	Branch	1	1	1	130				125.4	24.3	P	d	Slide is mis-labeled actual depth 3271', potentially leaked? Bubble renucleates below 30C
P3291	Arco Peck #-16	16-5S-7W	997.0	Wildcat	Branch	1	1	2	127						P	d	Slide is mis-labeled actual depth 3271', leaked after second heating run? Bubble did not come back after freezing
P3291	Arco Peck #-16	16-5S-7W	997.0	Wildcat	Branch	1	1	3	119	-23.0	-49	24.3			P	d	Slide is mis-labeled actual depth 3271',
P3291	Arco Peck #-16	16-5S-7W	997.0	Wildcat	Branch	2	1	1	79	-25.0		25.6	114.4	26.0	P	d	Slide is mis-labeled actual depth 3271', Bubble disappeared after first heating, bubble came back at -70C, Post freezing Th = 81.4,
P3291	Arco Peck #-16	16-5S-7W	997.0	Wildcat	Branch	2	1	2	105	-26.0		26.2			P	d	Slide is mis-labeled actual depth 3271',
P3291	Arco Peck #-16	16-5S-7W	997.0	Wildcat	Branch	2	1	3	119	-26.0		26.2			P	d	Slide is mis-labeled actual depth 3271',
P3291	Arco Peck #-16	16-5S-7W	997.0	Wildcat	Branch	2	1	4	108	-26.0		26.2			P	d	Slide is mis-labeled actual depth 3271',
P3291	Arco Peck #-16	16-5S-7W	997.0	Wildcat	Branch	2	1	5	112	-25.0	-63.8	25.6			P	d	Slide is mis-labeled actual depth 3271',
P3291	Arco Peck #-16	16-5S-7W	997.0	Wildcat	Branch	2	1	6	121	-25.7		26.0			P	d	Slide is mis-labeled actual depth 3271',
P3291	Arco Peck #-16	16-5S-7W	997.0	Wildcat	Branch	2	1	7	121	-26.5		26.5			P	d	Slide is mis-labeled actual depth 3271',

P3291	Arco Peck #-16	16-5S-7W	997.0	Wildcat	Branch	2	1	8	115	-25.5	-63.8	25.9			P	d	Slide is mis-labeled actual depth 3271',
P3291	Arco Peck #-16	16-5S-7W	997.0	Wildcat	Branch	3	1	1		-12.0		16.0		16.1	P	d	Freezing only. Slide is mis-labeled actual depth 3271', leaked after F1
P3291	Arco Peck #-16	16-5S-7W	997.0	Wildcat	Branch	3	1	2			-38.8				P	d	Freezing only. Slide is mis-labeled actual depth 3271',
P3291	Arco Peck #-16	16-5S-7W	997.0	Wildcat	Branch	3	1	4		-12.4		16.3			P	d	Freezing only. Slide is mis-labeled actual depth 3271', bubble nucleated after first freezing run
P3271	Arco Peck #-16	16-5S-7W	1003.1	Wildcat	Branch	1	1	1	126	-26.1		26.3	125.0	26.4	P	d	
P3271	Arco Peck #-16	16-5S-7W	1003.1	Wildcat	Branch	1	1	2	123	-25.2		25.7			P	d	
P3271	Arco Peck #-16	16-5S-7W	1003.1	Wildcat	Branch	1	1	4	126	-27.6		27.2			P	d	
P3271	Arco Peck #-16	16-5S-7W	1003.1	Wildcat	Branch	1	2	5	162	-26.5		26.5	160.4	26.1	P	d	Possible hydrohalite, melted at -8.3 after water ice
P3271	Arco Peck #-16	16-5S-7W	1003.1	Wildcat	Branch	1	2	6	160	-26.3		26.4			P	d	
P3271	Arco Peck #-16	16-5S-7W	1003.1	Wildcat	Branch	1	2	7	160	-24.9		25.5			P	d	

VITA

Regina Frances Dunseith

Candidate for the Degree of

Master of Science

Thesis: FLUID HISTORIES OF MIDDLE ORDOVICIAN FAULT-FRACTURE DOLOMITE OIL FIELDS OF THE SOUTHERN MICHIGAN BASIN

Major Field: Geology

Biographical:

Education:

Completed the requirements for the Master of Science in Geology at Oklahoma State University, Stillwater, Oklahoma in July, 2019.

Completed the requirements for the Bachelor of Science in Geology and Geophysics at University of Missouri-Rolla, Rolla, Missouri in 2009.

Experience:

Geosteering Geologist: Southwestern Energy Company	2009-2012
Geologist, Operations: Continental Resources, Inc.	2012-2015
Operations Team Lead: Continental Resources, Inc.	2015-2019
Supervisor, North Exploitation: Continental Resources, Inc.	2019-present

Professional Memberships:
Geological Society of America
Women's Energy Network